Effective rates from thermodynamically consistent coarse-graining of models for molecular motors with probe particles

Eva Zimmermann and Udo Seifert
II. Institut für Theoretische Physik, Universität Stuttgart, 70550 Stuttgart, Germany
(Received 18 July 2014; revised manuscript received 17 November 2014; published 17 February 2015)

Many single-molecule experiments for molecular motors comprise not only the motor but also large probe particles coupled to it. The theoretical analysis of these assays, however, often takes into account only the degrees of freedom representing the motor. We present a coarse-graining method that maps a model comprising two coupled degrees of freedom which represent motor and probe particle to such an effective one-particle model by eliminating the dynamics of the probe particle in a thermodynamically and dynamically consistent way. The coarse-grained rates obey a local detailed balance condition and reproduce the net currents. Moreover, the average entropy production as well as the thermodynamic efficiency is invariant under this coarse-graining procedure. Our analysis reveals that only by assuming unrealistically fast probe particles, the coarse-grained transition rates coincide with the transition rates of the traditionally used one-particle motor models. Additionally, we find that for multicyclic motors the stall force can depend on the probe size. We apply this coarse-graining method to specific case studies of the F_1-ATPase and the kinesin motor.

DOI: 10.1103/PhysRevE.91.022709 PACS number(s): 87.16.Nn, 05.40.−a, 05.70.Ln

I. INTRODUCTION

In many single-molecule experiments beads that are attached to molecular motors are used to infer properties of the motor protein from the analysis of the trajectory of these probe particles. In particular, external forces can be exerted on the motor via such a probe particle [1,2]. In the theoretical analysis of such assays, the motor is usually modelled as a particle hopping on a discrete state space with transitions governed by a master equation [3–8]. Alternatively, the so-called ratchet models combine continuous diffusive spatial motion with stochastic switching between different potentials corresponding to different chemical states [9,10]. These approaches often comprise only one particle explicitly, representing the motor. The contribution of external forces which in the experiments act on the motor only via the probe are then included in the transition rates [5,6,11–17] (or Langevin equation for the spatial coordinate [18,19]) of the motor particle directly. However, theoretical models that are used to reproduce the experimental observations should comprise at least two (coupled) degrees of freedom, one for the motor and one for the probe particle. Such models consisting of one degree of freedom hopping on a discrete state space representing the motor coupled to a continuously moving degree of freedom representing the probe are discussed in Refs. [20–27]. While multiparticle models are more precise and better represent the actual experimental setup, one-particle models are widely used toy models often applied to illustrate basic ideas.

Simplifying the description of systems consisting of many degrees of freedom with a concomitant large state space while still maintaining important properties is commonly known as coarse-graining. In the context of stochastic thermodynamics [28], various coarse-graining methods have been applied, e.g., lumping together states of a discrete state space among which transitions are fast [29–32], averaging over states for discrete [33] or continuous processes [32,34], eliminating single states from a network description [35–37], or eliminating slow (invisible) degrees of freedom [38–40]. It was found that, in general, coarse-graining has implications on the entropy production and, in particular [41], dissipation. In the context of biological systems and especially molecular motors, coarse-graining procedures mostly focus on eliminating selected states of the motor [37,42] or on reducing continuous (ratchet) models to discrete-state models [43–47].

In the present paper, we introduce a coarse-graining procedure that allows us to reduce molecular motor-bead models to effective one-particle models with discrete motor states with the external force acting directly on the effective motor particle. We eliminate the explicit dynamics of the probe particle completely still maintaining the correct local detailed balance condition for the effective motor transition rates and preserving the average currents of the system. As a main result, we find that the coarse-grained rates show a more complex force dependence than the usually assumed exponential behavior and a more complex concentration dependence than mass action law kinetics.

The paper is organized as follows. In Sec. II, we introduce our coarse-graining method on the basis of a simple motor-bead model with only one motor state and apply it to a model for the F_1-ATPase [26]. In Sec. III, we generalize the procedure to motor models with several internal states and apply it to both a refined model for the F_1-ATPase and to a kinesin model. A possible experimental implementation of our method is presented in Sec. IV. We show that entropy production and efficiency remain invariant under this coarse-graining procedure in Sec. V, discuss implications on the stall conditions in Sec. VI, and conclude in Sec. VII.

II. GENERAL ONE-STATE MOTOR MODEL

A. Explicit motor-bead dynamics

The general model for motor proteins with only one chemical state consists of one degree of freedom representing the motor which jumps between discrete states $n(t)$ separated by a distance d. The motor is coupled with the second degree of freedom representing the probe particle via some kind of

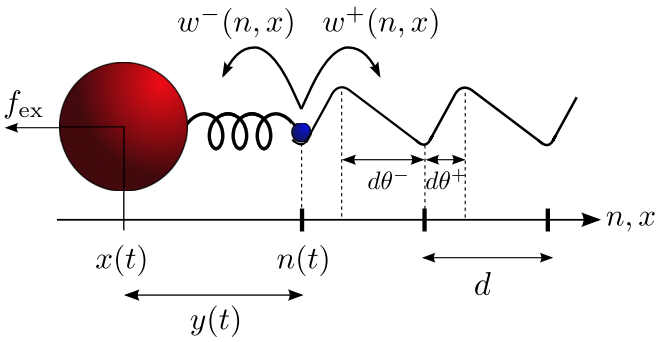

FIG. 1. (Color online) Schematic representation of a motor-bead model comprising a one-state motor (small blue sphere) attached via an elastic linker to the probe particle (large red sphere). An external force $f_{\rm ex}$ is applied to the bead. The transition rates of the motor are denoted by $w^+(n,x)$ and $w^-(n,x)$. The load-sharing factors θ^+ and θ^- indicate the position of an underlying unresolved potential barrier relative to the minimum of the free-energy landscape of the motor.

elastic linker, see Fig. 1 [26]. The motion of the probe particle with continuous coordinate $x(t)$ is described by an overdamped Langevin equation with friction coefficient γ and constant external force $f_{\rm ex}$,

$$\dot{x}(t) = [-\partial_x V(n-x) - f_{\rm ex}]/\gamma + \zeta(t), \tag{1}$$

including the potential energy of the linker $V(n-x)$ and thermal noise $\zeta(t)$ with correlations $\langle\zeta(t_2)\zeta(t_1)\rangle = 2\delta(t_2-t_1)/\gamma$. Throughout the paper, we set $k_BT = 1$. This choice implies that the product of force $f_{\rm ex}$ and distance d appearing in the figures below is measured in units of k_BT. The (instantaneous) distance between motor and probe is denoted by y. The system is characterized by the pair of variables (n,x) and is "bipartite" in these variables since transitions do not happen in both variables at the same time. The transition rates of the motor fulfill a local detailed balance (LDB) condition,

$$\frac{w^+(y)}{w^-(y+d)} = \exp[\Delta\mu - V(y+d) + V(y)]. \tag{2}$$

The free-energy change of the solvent $\Delta\mu \equiv \mu_T - \mu_D - \mu_P$ with $\mu_i = \mu_i^{\rm eq} + \ln(c_i/c_i^{\rm eq})$ and nucleotide concentrations c_i is associated with ATP turnover. The probability density $p(y)$ for the distance y obeys a Fokker-Planck-type equation,

$$\begin{aligned}\partial_t p(y) = {}& \partial_y\{[\partial_y V(y) - f_{\rm ex}]\, p(y) + \partial_y\, p(y)\}/\gamma \\ & + w^+(y-d)\, p(y-d) + w^-(y+d)\, p(y+d) \\ & - [w^+(y) + w^-(y)]\, p(y).\end{aligned} \tag{3}$$

For constant nucleotide concentrations, the system reaches a nonequilibrium stationary state (NESS) with constant average velocity,

$$\begin{aligned}v &\equiv d\int_{-\infty}^{\infty} p^s(y)[w^+(y) - w^-(y)]\, dy \\ &= \int_{-\infty}^{\infty} p^s(y)[\partial_y V(y) - f_{\rm ex}]/\gamma\, dy,\end{aligned} \tag{4}$$

and stationary distribution $p^s(y)$.

B. Coarse-graining procedure

In the coarse-grained description of the model we want to map the motor-bead system to one effective motor particle hopping between states separated by d. We thus have to eliminate the x coordinate from the (n,x) description resulting in a system characterized only by n.

For the coarse-grained model, we impose the following conditions. The coarse-grained transition rates $\Omega^\pm$ which advance the effective particle by d should obey a LDB condition,

$$\frac{\Omega^+}{\Omega^-} = \exp[\Delta\mu - f_{\rm ex}d], \tag{5}$$

as the force is now assumed to act directly on the effective motor particle. Furthermore, we require that the coarse-grained particle moves with the same average velocity in the steady state as the motor and the probe in the original model, i.e.,

$$v = d(\Omega^+ - \Omega^-). \tag{6}$$

Solving the linear system of Eqs. (5) and (6) yields the coarse-grained rates

$$\Omega^+ = \frac{v\exp[\Delta\mu - f_{\rm ex}d]/d}{\exp[\Delta\mu - f_{\rm ex}d] - 1}, \tag{7}$$

$$\Omega^- = \frac{v/d}{\exp[\Delta\mu - f_{\rm ex}d] - 1}. \tag{8}$$

The coarse-grained rates can be interpreted as effective transition rates that correspond to a transition process after which both particles, motor and probe, have advanced a distance $\pm d$. In principle, there are (for any y) many possible displacement processes to advance both particles by d, including ones with l forward and $l-1$ backward motor jumps. The coarse-grained rate corresponds to the rate with which one such effective displacement will happen.

In general, the coarse-grained rates depend (via v) on all model parameters, including the friction coefficient of the probe particle and the specific potential of the linker. If one had chosen coarse-grained rates by just averaging over the positions of the probe particle, i.e., by

$$\langle w^\pm\rangle = \int_{-\infty}^{\infty} p^s(y) w^\pm(y)\, dy, \tag{9}$$

one would have obtained rates that yield the correct average velocity but do not fulfill the LDB condition, as discussed in Sec. II E below.

For a more explicit analysis, we must specify the forward and backward rates of the motor. We choose [26]

$$w^+(y) = w_0\exp[\mu^+ - V(y+d\theta^+) + V(y)], \tag{10}$$

$$w^-(y) = w_0\exp[\mu^- - V(y-d\theta^-) + V(y)], \tag{11}$$

where θ^+ and θ^- are the load-sharing factors with $\theta^+ + \theta^- = 1$ and $\mu^+ = \mu_T$, $\mu^- = \mu_D + \mu_P$. We assume an exponential dependence of the transition rates on the potential difference of the linker according to Kramers's theory. This exponential dependence on the potential difference is similar to one-particle models where the rates of the motor typically depend exponentially on the external force with a corresponding load-sharing factor [3,5].

C. Time-scale separation

In this section, we will investigate under which conditions the coarse-grained rates (7) and (8) can be expressed using a single exponential dependence on the external force as typically assumed for mechanical transitions within one-particle models [3,5].

Inserting Eqs. (10) and (11) in Eq. (3) in the NESS shows that the contribution due to motor jumps is weighted with a (dimensionless) prefactor,

$$\varepsilon \equiv w_0 \exp\left[\mu_T^{\mathrm{eq}}\right] d^2 \gamma. \tag{12}$$

Here $w_0 \exp[\mu_T^{\mathrm{eq}}]$ determines the time scale of the transitions of the motor while γd^2 determines the time scale of the dynamics of the probe particle. The latter is mainly governed by the size of the bead and the step size of the motor, whereas $w_0 \exp[\mu_T^{\mathrm{eq}}]$ is determined by the attempt frequency and also by the absolute nucleotide concentrations.

If the dynamics of the bead is much faster than the transitions of the motor, time-scale separation holds with $\varepsilon \to 0$ [31,48]. In this limit of fast bead relaxation, denoted throughout by a caret, the stationary solution of Eq. (3) in the NESS becomes

$$\hat{p}^s(y) = \exp[-V(y) + f_{\mathrm{ex}} y]/\mathcal{N} \tag{13}$$

with $\mathcal{N} \equiv \int_{-\infty}^{\infty} \exp[-V(y) + f_{\mathrm{ex}} y] dy$. The average velocity is then given by

$$\begin{aligned} \hat{v} &= d \int_{-\infty}^{\infty} \hat{p}^s(y)[w^+(y) - w^-(y)] dy \\ &= d w_0 (e^{\mu_T - f_{\mathrm{ex}} d\theta^+} - e^{\mu_D + \mu_P + f_{\mathrm{ex}} d\theta^-}). \end{aligned} \tag{14}$$

This expression inserted into Eqs. (7) and (8) yields

$$\hat{\Omega}^+ = w_0 e^{\mu_T - f_{\mathrm{ex}} d\theta^+}, \tag{15}$$

$$\hat{\Omega}^- = w_0 e^{\mu_D + \mu_P + f_{\mathrm{ex}} d\theta^-}, \tag{16}$$

independent of any specific linker potential $V(y)$. Since this force dependence is purely exponential with the correct load-sharing factor, these expressions represent exactly the rates typically used in one-particle models. We notice that within this approximation $\Omega^+ = \langle w^+(y) \rangle$ and $\Omega^- = \langle w^-(y) \rangle$ holds true, which is in agreement with other coarse-graining procedures in the time-scale separation limit, e.g., Refs. [31–33].

Note that only transition rates of the motor whose dependence on the linker potential is chosen accordingly in the Kramers form [Eqs. (10) and (11)] lead generically to consistent coarse-grained and averaged rates when using the fast-bead limit of $p^s(y)$.

D. Example: F_1-ATPase

In general, a strong time-scale separation between motor and probe is not necessarily realistic. In this case, Eq. (3) must be solved numerically. We will use the model introduced in Ref. [26], see Fig. 1, with a harmonic potential $V(y) = \kappa y^2/2$ as a simple example to illustrate our coarse-graining procedure.

In Fig. 2, the results for Ω^+ and Ω^- are shown for various values of the friction coefficient γ. With decreasing γ, the rates approach their corresponding fast-bead limits, $\hat{\Omega}^+$ and $\hat{\Omega}^-$. These values are upper bounds because decreasing γ implies smaller probe particles which exert less drag on the motor. For finite γ, the coarse-grained rates do not show a single exponential dependence on f_{ex} over the whole range of external forces. Such a dependence, however, is usually assumed to hold within one-particle models. Moreover, the coarse-grained rates depend on γ, which is a parameter not incorporated explicitly in many one-particle models.

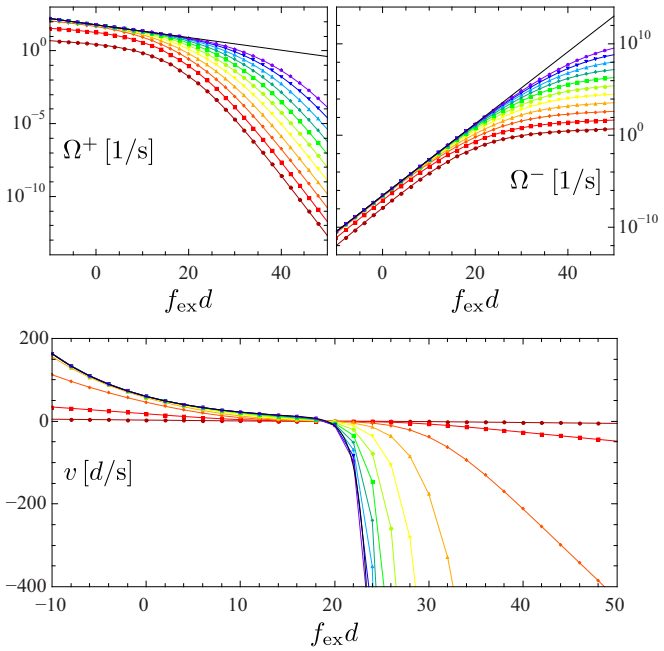

FIG. 2. (Color online) Coarse-grained rates Ω^+ and Ω^- (top) and average velocity (bottom) as functions of $f_{\mathrm{ex}}d$ for various friction coefficients γ in the range $5\ \mathrm{s}/d^2 \geqslant \gamma \geqslant 5 \times 10^{-10}\ \mathrm{s}/d^2$ (from bottom to top). With decreasing γ, the rates and the velocity approach the corresponding fast-bead limit (solid black lines). Parameters: $\kappa = 40\ d^{-2}$, $c_T = c_D = 2 \times 10^{-6}$ M, $c_P = 10^{-3}$ M, $\Delta\mu = 19$, $\theta^+ = 0.1$, $w_0 \exp[\mu_T^{\mathrm{eq}}]/c_T^{\mathrm{eq}} = 3 \times 10^7\ (\mathrm{Ms})^{-1}$.

The experimentally accessible values of γ cover a wide range of the values chosen in Fig. 2. A dimer of polystyrene beads ($\simeq 280$ nm) as used in Refs. [49–52] corresponds to $\gamma = 0.5\ \mathrm{s}/d^2$ [red (dark gray) line with squares] while a 40-nm-gold particle [52–54] corresponds to $\gamma = 5 \times 10^{-4}\ \mathrm{s}/d^2$ [yellow (light gray) line with triangles]. Especially for large external forces, the coarse-grained rates deviate strongly from their asymptotic values even for a probe as small as the gold particle.

The average velocity as shown in Fig. 2 also strongly depends on the friction coefficient of the probe particle, especially for large external forces. In this regime, for large γ, the velocity is dominated by the friction experienced by the probe while for small γ the probe relaxes almost immediately and the velocity is dominated by the time scale of the motor jumps.

Another option to reach the fast-bead limit is to use very small nucleotide concentrations. In Fig. 3, we show the coarse-grained rates for various ATP and ADP concentrations. With decreasing nucleotide concentration (at fixed $\Delta\mu$), the rates approach the asymptotic $\hat{\Omega}^+$ and $\hat{\Omega}^-$. However, it is very hard to do experiments at concentrations smaller than $\simeq 10^{-7}$ M as jumps of the motor are then very rare.

In Fig. 2 and in Fig. 3 the dependence of the coarse-grained rates on the external force exhibits two different regimes.

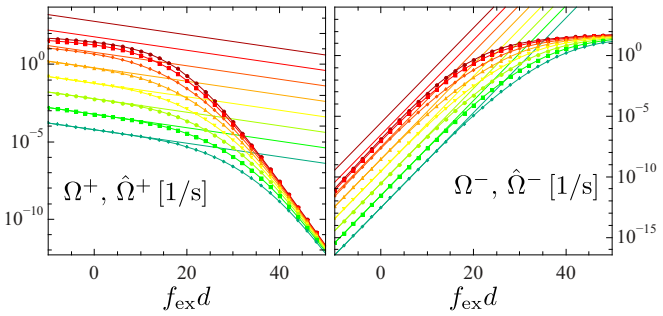

FIG. 3. (Color online) Coarse-grained rates Ω^+ and Ω^- as functions of $f_{\rm ex}d$ for various c_T, c_D in the range 2×10^{-5} M $\geqslant c_T, c_D \geqslant 2\times10^{-12}$ M (from top to bottom). With decreasing c_T,c_D, the rates approach the fast-bead limits $\hat{\Omega}^+$ and $\hat{\Omega}^-$ (straight lines). Parameters: $\kappa = 40\,d^{-2}$, $\gamma = 0.5$ s$/d^2$, $c_P = 10^{-3}$ M, $\Delta\mu = 19$, $\theta^+ = 0.1$, $w_0 \exp[\mu_T^{\rm eq}]/c_T^{\rm eq} = 3\times10^7$ (Ms)$^{-1}$.

Up to values of the external force of roughly $15/d$, the coarse-grained rates can be well approximated by a single exponential dependence on $f_{\rm ex}$ with the same slope as in the fast-bead limit, $d\theta^+$ or $d\theta^-$, respectively. However, for large γ and large c_T, even in this regime, the absolute values of the coarse-grained rates deviate up to two orders of magnitude from their fast-bead approximation. For such parameters, assuming a monoexponential dependence on $f_{\rm ex}$ with the above slope would not be appropriate either.

For large external forces, all coarse-grained rates deviate significantly from their fast-bead limits. We find again a monoexponential decay for Ω^+ but now with slope $-d$, whereas Ω^- grows only linearly with increasing $f_{\rm ex}$. This so far unaccounted for behavior can be understood by considering the limit $f_{\rm ex}\to\infty$ as discussed in detail in the appendix. The crossover from one regime to the other occurs beyond the stall force $f_{\rm ex} = \Delta\mu/d$.

In summary, we find that for the F_1-ATPase under realistic experimental conditions the rates in a coarse-grained description comprising only one effective particle that satisfy the LDB condition Eq. (5) and reproduce the correct average velocity v cannot be written in the form of a single exponential dependence on the external force.

E. Comparison of coarse-grained with averaged rates

Instead of defining the coarse-grained rates according to Eqs. (7) and (8), one might be tempted to use the averaged rates (9) as a definition for the coarse-grained rates. In Fig. 4, we show the averaged rates of our F_1-ATPase model as well as their ratio corresponding to the LDB condition. We find that both $\langle w^+\rangle$ and $\langle w^-\rangle$ (for the latter less visible in the plot) exhibit nonmonotonic dependence on the external force. For external forces slightly larger than the stall force, $\langle w^+\rangle$ increases with increasing $f_{\rm ex}$ due to the fact that in this region the system moves backward with motor jumps following the probe which leads to a peak at small y in $p^s(y)$. On the other hand, $\langle w^-\rangle$ exhibits a minimum around stall conditions for large γ since in this region, $p^s(y)$ misses a peak at large $y\simeq 1$.

A severe issue appears regarding the LDB condition. The corresponding ratio of the averaged rates is also plotted in Fig. 4 where it can be clearly seen that the LDB condition is not fulfilled (except in the fast-bead limit).

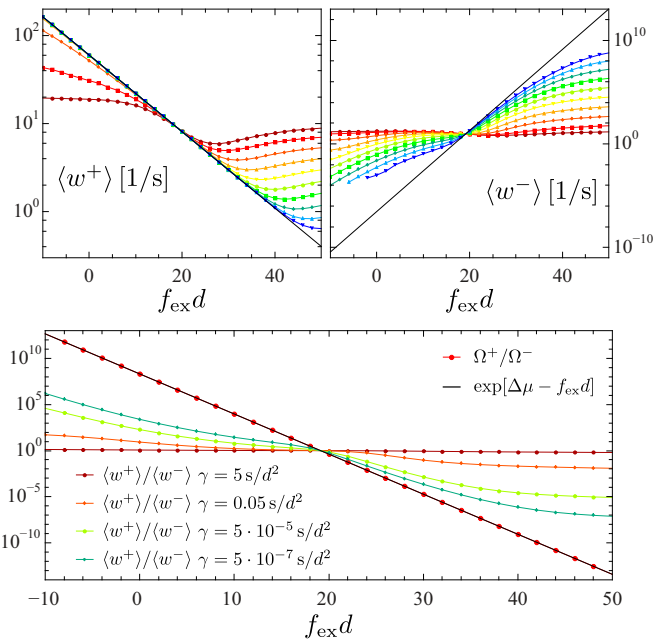

FIG. 4. (Color online) Top: Average rates $\langle w^+\rangle$ and $\langle w^-\rangle$ as functions of $f_{\rm ex}d$ for various γ in the range $5\ {\rm s}/d^2 \geqslant \gamma \geqslant 5\times10^{-9}\ {\rm s}/d^2$. With decreasing γ, the rates approach $\hat{\Omega}^+$, $\hat{\Omega}^-$ (solid black lines). Bottom: Ratio of $+$ and $-$ rates. In contrast to Ω^+, Ω^- (large red dots), the averaged motor rates do not fulfill the LDB condition (solid black line). The parameters are the same as in Fig. 2.

F. Without external force

Even though we have motivated this paper by emphasizing that external forces are typically applied to probe particles, it should be obvious that our approach holds true for molecular motors transporting cargo subject to Stokes friction in the absence of external forces.

For one-particle models, the friction coefficient of the probe cannot be taken into account explicitly. One rather has to incorporate the drag effect of the bead into the motor rates [46]. If one wants to analyze experimental data obtained from probe particles of different sizes, one then has to use different values of the motor rates for each data set.

For the rather dilute solutions used in experiments in Refs. [49,51,55] one generally assumes that the motor dynamics is subject to mass action law kinetics, i.e., that the transition rates depend linearly on the corresponding concentration of nucleotides. Obviously, this linear dependence holds for all concentrations and beads of all sizes for one-particle models. When keeping c_D and c_P fixed, the average velocity of a one-state motor will show a purely linear dependence on c_T.

The experimental analysis of the average velocity of the F_1-ATPase as function of c_T (for fixed c_D, c_P) reveals a saturation of the velocity for large ATP concentrations which sets in earlier for large beads [53]. While such a saturation is usually attributed to the hydrolysis step, we find that a sublinear dependence of the velocity can also be caused by the drag of the probe particle.

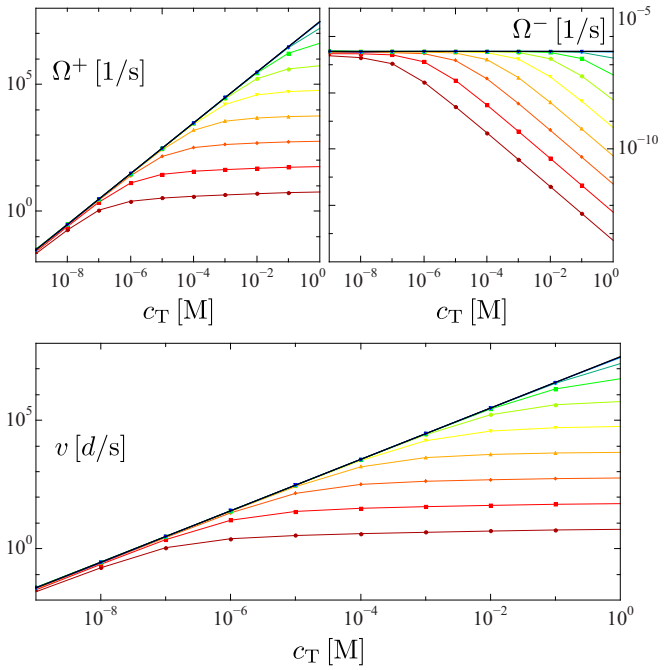

FIG. 5. (Color online) Coarse-grained rates Ω^+ and Ω^- (top) and average velocity (bottom) for various γ and $f_{ex} = 0$ as functions of c_T. Since c_D and c_P are fixed, $\Delta\mu$ also increases with c_T. The rates and the velocity approach the fast-bead approximation (solid black lines). Parameters: $c_D = 2 \times 10^{-6}$ M, $c_P = 1 \times 10^{-3}$ M, $\kappa = 40\ d^{-2}$, $\theta^+ = 0.1$, $w_0 \exp[\mu_T^{eq}]/c_T^{eq} = 3 \times 10^7$ (Ms)$^{-1}$, γ in the range $5\ \text{s}/d^2 \geqslant \gamma \geqslant 5 \times 10^{-9}\ \text{s}/d^2$ (from bottom to top).

In Fig. 5, the coarse-grained rates as well as the velocity are shown as a function of the ATP concentration. With decreasing γ, the coarse-grained rates approach the fast-bead limit and the mass action law kinetics. The velocity is then linear in c_T as in a one-particle model. For large γ, eliminating the cargo by coarse-graining yields coarse-grained rates that are not linear in the concentrations although the motor rates are still subject to mass action law kinetics. Moreover, the velocity then exhibits a sublinear dependence reminiscent of the typical saturation effect for large c_T.

G. Comparison of full and coarse-grained trajectories

Trajectories of motor and probe generated by a simulation of the complete model of the F_1-ATPase are shown in Fig. 6. Additionally, Fig. 6 contains a trajectory obtained from simulating the corresponding coarse-grained model. The average velocity of both models is the same [by definition, see Eq. (6)], whereas the coarse-grained model produces trajectories that are "more random." This behavior occurs since the coarse-grained rates are constant (for fixed parameters) and produce a simple biased random walk. The motor transition rates of the complete model, however, depend on the actual position of the probe and are therefore implicitly time dependent. Since fast successive motor jumps are suppressed, the trajectory of the complete model is less random [21,56].

The influence of parameters like the probe size or the ATP concentration on the dynamics is visible in the bottom panels of Fig. 6. While the average velocity is almost the same,

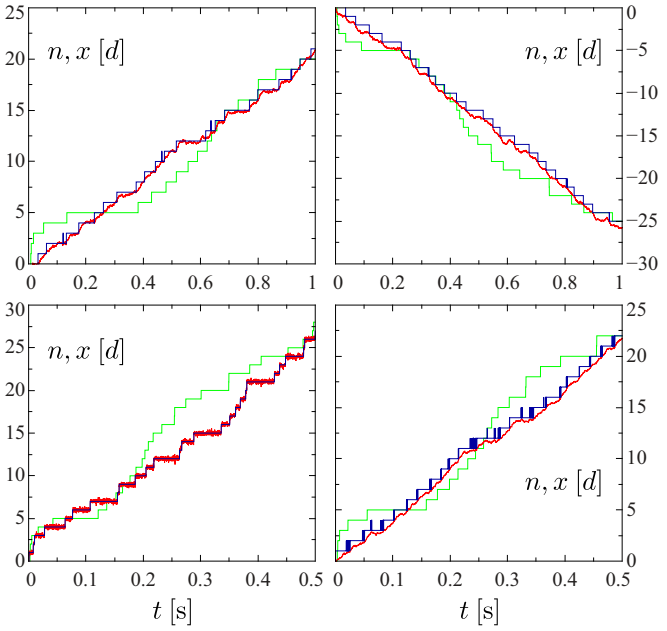

FIG. 6. (Color online) Trajectories of the one-state model for the F_1-ATPase for several parameter sets obtained from simulations. The trajectory of the detailed model (motor: steplike blue lines; probe: fluctuating red lines) is shown together with a trajectory of its corresponding coarse-grained model [green (light gray)]. Parameters: $\kappa = 40\ d^{-2}$, $\theta^+ = 0.1$, $w_0 \exp[\mu_T^{eq}]/c_T^{eq} = 3 \times 10^7$ (Ms)$^{-1}$, $\gamma = 0.5\ \text{s}/d^2$, $f_{ex} = 0$, $c_T = c_D = 2 \times 10^{-6}$ M, $c_P = 0.001$ M (top left); $\gamma = 0.5\ \text{s}/d^2$, $f_{ex} = 40\ d^{-1}$, $c_T = c_D = 2 \times 10^{-6}$ M, $c_P = 0.001$ M (top right); $\gamma = 0.005\ \text{s}/d^2$, $f_{ex} = 0$, $c_T = c_D = 2 \times 10^{-6}$ M, $c_P = 0.001$ M (bottom left); $\gamma = 0.5\ \text{s}/d^2$, $f_{ex} = 0$, $c_T = 0.001$ M, $c_D = 2 \times 10^{-6}$ M, $c_P = 0.001$ M (bottom right).

the trajectories of the complete model differ significantly. Using a small probe with a small friction coefficient, the probe relaxes to the potential minimum of the linker before the next motor jump occurs, whereas the large probe cannot relax [25]. Large ATP concentrations induce many forward and successive backward motor jumps that are absent at lower ATP concentrations. These details are not captured in the coarse-grained trajectories.

III. MOTOR MODELS WITH SEVERAL INTERNAL STATES

A. Explicit motor-bead dynamics and coarse-graining procedure

In this section, we will generalize the model taking into account several different internal states of the motor labeled by i. The motor states represent the nodes and the transitions the edges of a network. Transitions between the motor states i and j change the free energy by

$$\Delta F_{ij}^{\alpha} \equiv F_j - F_i - \Delta\mu_{ij}^{\alpha}, \tag{17}$$

where $F_j - F_i$ is the free-energy difference of the internal states of the motor and $\Delta\mu_{ij}^{\alpha} = -\Delta\mu_{ji}^{\alpha}$ is the free-energy change of the solvent. Depending on the transition, $\Delta\mu_{ij}^{\alpha}$ is given by μ_T, μ_D, μ_P or any combination thereof or 0. Transitions may also advance the motor a distance $d_{ij}^{\alpha} = -d_{ji}^{\alpha}$.

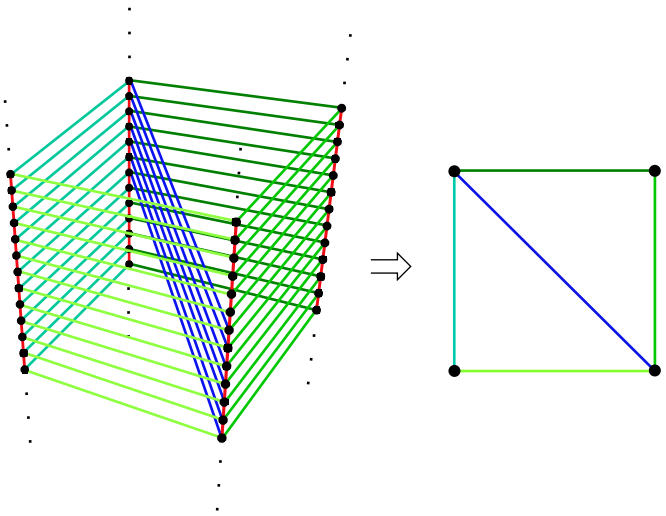

FIG. 7. (Color online) Network representation of a motor-bead model with four internal motor states and discretized state space of the probe particle (left). Each row of black dots represents one motor state while the dots themselves represent specific distances y accessible to the probe particle (via the vertical red lines) within the same motor state. Transitions between motor states either leave y the same (horizontal green lines) or can advance the motor by d_{ij}^{α} and change y (diagonal blue lines). The top view of this network corresponds to the coarse-grained version of this model (right).

Since we allow for several transitions connecting two states, we assign an additional index α to the transitions indicating which link between i and j is used. An example for the network of a full system comprising motor and probe particle is shown in Fig. 7, where the state space of the probe is discretized for better presentation.

The Fokker-Planck-type equation for such models is given by

$$\partial_t p_i(y) = \partial_y\{[\partial_y V(y) - f_{\rm ex}]p_i(y) + \partial_y p_i(y)\}/\gamma + \sum_{j,\alpha}\left[w_{ji}^{\alpha}\left(y + d_{ij}^{\alpha}\right)p_j\left(y + d_{ij}^{\alpha}\right) - w_{ij}^{\alpha}(y)p_i(y)\right] \tag{18}$$

with transition rates of the motor that obey a LDB condition

$$\frac{w_{ij}^{\alpha}(y)}{w_{ji}^{\alpha}\left(y + d_{ij}^{\alpha}\right)} = \exp\left[-\Delta F_{ij}^{\alpha} - V\left(y + d_{ij}^{\alpha}\right) + V(y)\right]. \tag{19}$$

The coarse-grained version of such a model should take into account the different states of the motor as well as the several possible α transitions between i and j. Thus, the motor network (including all motor cycles) should be conserved under coarse-graining. To account for the several internal states, we require that the coarse-grained rates should obey a LDB condition and the operational current [57] from motor state i to motor state j via edge α should be conserved. The operational current is the sum over all y-dependent net transition currents that contribute to the transition $i \to j$. Conserving the operational currents corresponds to the condition of reproducing the correct mean velocity for the one-state model. The above conditions read

$$\frac{\Omega_{ij}^{\alpha}}{\Omega_{ji}^{\alpha}} = \exp\left[-\Delta F_{ij}^{\alpha} - f_{\rm ex}d_{ij}^{\alpha}\right] \tag{20}$$

and

$$P_i\Omega_{ij}^{\alpha} - P_j\Omega_{ji}^{\alpha} = j_{ij}^{\alpha} \tag{21}$$

with the operational current

$$j_{ij}^{\alpha} \equiv \int_{-\infty}^{\infty}\left[p_i(y)w_{ij}^{\alpha}(y) - p_j\left(y + d_{ij}^{\alpha}\right)w_{ji}^{\alpha}\left(y + d_{ij}^{\alpha}\right)\right]dy = -j_{ji}^{\alpha} \tag{22}$$

and the marginal distribution

$$P_i = \int_{-\infty}^{\infty} p_i(y)\,dy. \tag{23}$$

These equations can be solved for Ω_{ij}^{α} and Ω_{ji}^{α} using simple algebra which yields the rates

$$\Omega_{ij}^{\alpha} = j_{ij}^{\alpha}\frac{\exp\left[-\Delta F_{ij}^{\alpha} - f_{\rm ex}d_{ij}^{\alpha}\right]}{P_i\exp\left[-\Delta F_{ij}^{\alpha} - f_{\rm ex}d_{ij}^{\alpha}\right] - P_j}, \tag{24}$$

$$\Omega_{ji}^{\alpha} = j_{ij}^{\alpha}\frac{1}{P_i\exp\left[-\Delta F_{ij}^{\alpha} - f_{\rm ex}d_{ij}^{\alpha}\right] - P_j}. \tag{25}$$

In principle, it is sufficient to use only Eq. (24), since Ω_{ji}^{α} takes exactly this form with $j_{ij}^{\alpha} = -j_{ji}^{\alpha}, \Delta F_{ij}^{\alpha} = -\Delta F_{ji}^{\alpha}$, and $d_{ij}^{\alpha} = -d_{ji}^{\alpha}$. This equivalent procedure would be more symmetric and treat all transition rates on an equal footing but the LDB condition is then less obvious. Note that without the LDB condition (20), the stated conditions of P_i and j_{ij}^{α} would also be compatible with coarse-grained rates like the ones in, e.g., Refs. [31,33].

Transitions whose rates are independent of the linker elongation y and hence have $d_{ij}^{\alpha} = 0$ retrieve their original rate constants through this coarse-graining procedure. For such a transition, j_{ij}^{α} is given by

$$j_{ij}^{\alpha} = P_i w_{ij}^{\alpha} - P_j w_{ji}^{\alpha} \tag{26}$$

with rates fulfilling the LDB condition $w_{ij}^{\alpha}/w_{ji}^{\alpha} = \exp[-\Delta F_{ij}^{\alpha}]$. Inserting j_{ij}^{α} into Eqs. (24) and (25) and using the LDB condition and $d_{ij}^{\alpha} = 0$ immediately yields

$$\Omega_{ij}^{\alpha} = w_{ij}^{\alpha}, \quad \Omega_{ji}^{\alpha} = w_{ji}^{\alpha}. \tag{27}$$

Transitions with rates depending on y but with $d_{ij}^{\alpha} = 0$ have coarse-grained rates that depend on $f_{\rm ex}$ only implicitly via j_{ij}^{α} and $P_{i,j}$ as will be discussed in Sec. III D for the chemical transition rates of kinesin.

The rates determined from the LDB condition Eq. (20), the populations P_i, and the operational currents are algebraically consistent with the fact that a full set of rates Ω_{ij}^{α} will uniquely determine the populations P_i on the coarse-grained network. Consistency can be seen by integrating the Fokker-Planck equation (18) over y, yielding the coarse-grained master equation

$$\partial_t P_i = \sum_{j,\alpha} j_{ji}^{\alpha} = \sum_{j,\alpha} P_j\Omega_{ji}^{\alpha} - P_i\Omega_{ij}^{\alpha}, \tag{28}$$

whose stationary solution in the NESS can be expressed as a function of the rates Ω_{ij}^{α} [57,58]. Thus, the expression of any current observable in terms of the operational currents is consistent with its expression in terms of cycle currents on the coarse-grained network.

B. Time-scale separation

Similarly to the one-state model, we explore the consequences of a putative time-scale separation between the dynamics of motor and probe for each motor transition. In the limit $\gamma \to 0$ (formally equivalent to $\varepsilon \to 0$ but here one would have several ε_{ij} within the Fokker-Planck equation and all go to 0) the solution of Eq. (18) in the NESS becomes, analogously to Refs. [29,32],

$$\hat{p}_i^s(y) = \hat{P}_i \exp[-V(y) + f_{\rm ex} y]/\mathcal{N}. \tag{29}$$

The marginal distribution can be obtained using Eq. (18) with its solution for fast bead relaxation,

$$\begin{aligned}\partial_t \hat{P}_i &= \int_{-\infty}^{\infty} \partial_t \hat{p}_i^s(y)\, dy \\ &= \sum_{j,\alpha} \left(\hat{P}_j \langle w_{ji}^{\alpha}\rangle_y - \hat{P}_i \langle w_{ij}^{\alpha}\rangle_y\right) = \sum_{j,\alpha} \hat{j}_{ji}^{\alpha} = 0.\end{aligned} \tag{30}$$

For Kramers-type transition rates like Eqs. (10) and (11),

$$w_{ij}^{\alpha}(y) = k_{ij}^{\alpha} \exp\left[\mu_{ij}^{\alpha,+} - V\left(y + d_{ij}^{\alpha}\theta_{ij}^{\alpha,+}\right) + V(y)\right], \tag{31}$$

$$w_{ji}^{\alpha}(y) = k_{ji}^{\alpha} \exp\left[\mu_{ij}^{\alpha,-} - V\left(y - d_{ij}^{\alpha}\theta_{ij}^{\alpha,-}\right) + V(y)\right], \tag{32}$$

with $\mu_{ij}^{\alpha,+} - \mu_{ij}^{\alpha,-} = \Delta\mu_{ij}^{\alpha}$ and $k_{ij}^{\alpha}/k_{ji}^{\alpha} = \exp[-F_j + F_i]$, the y-averaged rates $\langle w_{ij}^{\alpha}\rangle_y$ and $\langle w_{ji}^{\alpha}\rangle_y$ become

$$\langle w_{ij}^{\alpha}\rangle_y = k_{ij}^{\alpha} \exp\left[\mu_{ij}^{\alpha,+} - f_{\rm ex} d_{ij}^{\alpha}\theta_{ij}^{\alpha,+}\right], \tag{33}$$

$$\langle w_{ji}^{\alpha}\rangle_y = k_{ji}^{\alpha} \exp\left[\mu_{ij}^{\alpha,-} + f_{\rm ex} d_{ij}^{\alpha}\theta_{ij}^{\alpha,-}\right]. \tag{34}$$

The change of chemical free energy $\Delta\mu_{ij}^{\alpha}$ is split into $\mu_{ij}^{\alpha,+}$ and $\mu_{ij}^{\alpha,-}$, indicating that both directions of the transition can involve binding and release of the chemical species that account for $\Delta\mu_{ij}^{\alpha}$. The free-energy change arising from changing the motor state, $F_j - F_i$, is incorporated in the attempt frequencies k_{ij}^{α} of the corresponding states. Inserting the operational current in the form of Eq. (30) with these averaged rates, simple calculus shows that the coarse-grained rates (24) and (25) reduce to

$$\hat{\Omega}_{ij}^{\alpha} = k_{ij}^{\alpha} \exp\left[\mu_{ij}^{\alpha,+} - f_{\rm ex} d_{ij}^{\alpha}\theta_{ij}^{\alpha,+}\right], \tag{35}$$

$$\hat{\Omega}_{ji}^{\alpha} = k_{ji}^{\alpha} \exp\left[\mu_{ij}^{\alpha,-} + f_{\rm ex} d_{ij}^{\alpha}\theta_{ij}^{\alpha,-}\right], \tag{36}$$

which is again consistent with transition rates of one-particle models that assume a purely exponential dependence on the external force.

C. Example: F_1-ATPase with intermediate step

1. With external force

The 120° step of the F_1-ATPase is known to consist of a 90° and a 30° substep [53]. Such a stepping behavior can be modelled with a unicyclic motor with two internal states. A schematic representation of a system comprising a probe particle and a motor with two internal states is shown in Fig. 8. The two different pathways for transitions between the states 1 and 2 correspond to the 90° and 30° substeps of the F_1-ATPase, respectively.

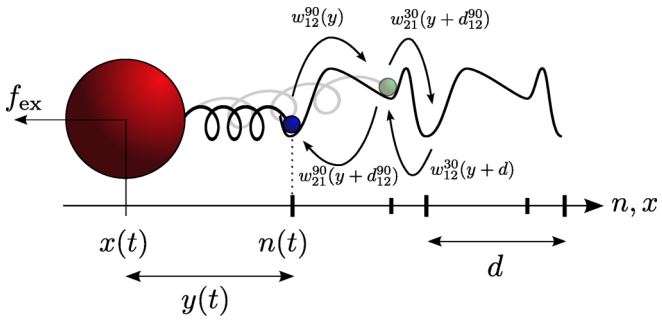

FIG. 8. (Color online) Schematic representation of a motor-bead model for the F_1-ATPase with two internal states of the motor, 1 [blue (dark gray)] and 2 [pale green (light gray)]. Transition between states 1 to 2 corresponding to the 90° (30°) substep are labeled with superscript 90 (30). The transition rates are chosen accordingly from Eqs. (31) and (32).

Like in Sec. II D for the one-state model, we examine the coarse-grained rates for the 90° and 30° steps and the velocity which are shown in Fig. 9. Similarly to the 120° scenario, the rates approach their fast-bead limit with decreasing γ.

As in the one-step model, the dependence of the coarse-grained rates on the external force shows two regimes. For small external forces, the rates can be well approximated by a single exponential dependence on $f_{\rm ex}$ with slope $\pm d_{ij}^{\alpha}\theta_{ij}^{\alpha,\pm}$ in most cases. For large probe particles, however, the rates neither match the absolute value nor show monoexponential dependence on $f_{\rm ex}$ with the above slope. For large forces, the forward rates decay faster, whereas the backward rates grow more slowly than in the fast-bead limit.

Concerning the average velocity, strong deviations from the fast-bead limit occur only for the largest friction coefficients. Using small beads, the force-velocity relation resulting from our coarse-graining procedure coincides well with the one obtained from a one-particle model due to the fact that the velocity involves only differences of the rates multiplied with the marginal distribution rather than the rates themselves. For large external forces and small γ, the velocity is significantly smaller than in the one-state model since the motor has to take two successive steps to cover the full d. The force-velocity relations for the two-state as well as for the one-state model reproduce very well the experimentally determined force-velocity relation from Ref. [51] for the corresponding value of the friction coefficient γ.

The limiting cases $f_{\rm ex} \to \pm\infty$ are more involved here than in the one-state model since one has to account for the dependence of the P_i's on the external force. However, as long as the P_j's do not decay faster than $\exp[-f_{\rm ex} d_{ij}^{\alpha}]$, it is still possible to approximate the rates (24) and (25) by

$$\Omega_{ij}^{\alpha} \approx -j_{ij}^{\alpha} \exp\left[-\Delta F_{ij}^{\alpha} - f_{\rm ex} d_{ij}^{\alpha}\right] / P_j, \tag{37}$$

$$\Omega_{ji}^{\alpha} \approx -j_{ij}^{\alpha} / P_j, \tag{38}$$

since P_i is bounded by 1.

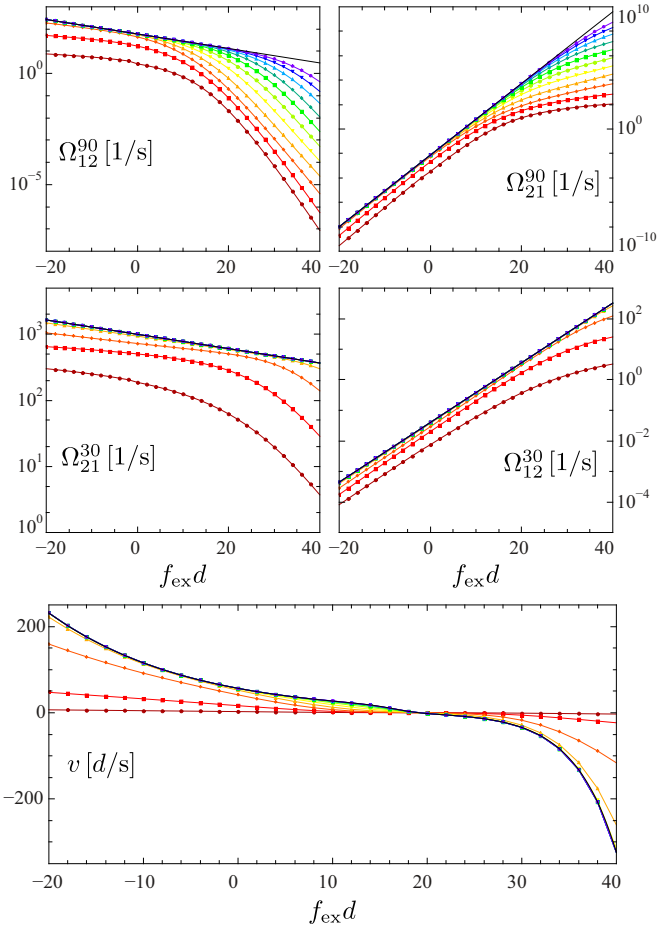

FIG. 9. (Color online) Coarse-grained rates for the 90° (top) and the 30° (center) substep and average velocity (bottom) as functions of $f_{\rm ex}d$ for various γ in the range $5\,{\rm s}/d^2 \geqslant \gamma \geqslant 5\times10^{-10}\,{\rm s}/d^2$ (from bottom to top). With decreasing γ, the rates and the velocity approach their corresponding fast-bead limit (solid black lines). Parameters: $\kappa = 40\,d^{-2}$, $c_T = c_D = 2\times10^{-6}$ M, $c_P = 10^{-3}$ M, $\theta^+_{90,30} = 0.1$, $k^{90}_{12}\exp[\mu^{\rm eq}_T]/c^{\rm eq}_T = 3\times10^7\,({\rm Ms})^{-1}$, $k^{90}_{21}\exp[\mu^{\rm eq}_D]/c^{\rm eq}_D = 3667.5\,({\rm Ms})^{-1}$, $k^{30}_{21} = 1000\,{\rm s}^{-1}$, $k^{30}_{12}\exp[\mu^{\rm eq}_P]/c^{\rm eq}_P = 40\,({\rm Ms})^{-1}$. The attempt frequencies are chosen on the basis of Refs. [53,54] where very small probe particles have been used.

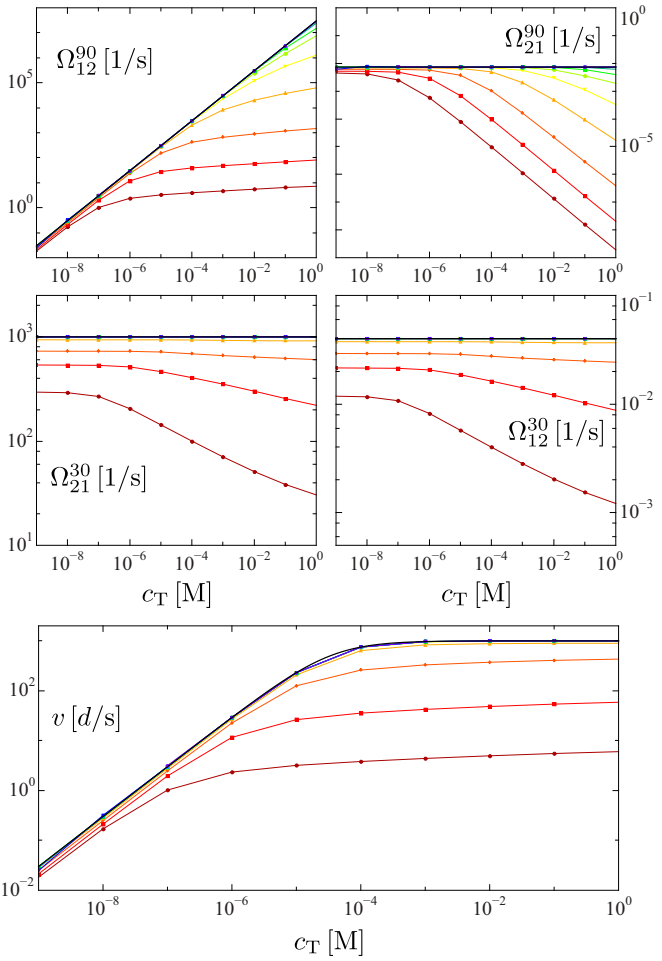

FIG. 10. (Color online) Coarse-grained rates for the 90° (top) and the 30° (center) substep and average velocity (bottom) for various γ and $f_{\rm ex} = 0$ as functions of c_T. Since c_D and c_P are fixed, $\Delta\mu$ also increases with c_T. The rates and the velocity approach the fast-bead approximation (solid black lines). Parameters: $c_D = 2\times10^{-6}$ M, $c_P = 1\times10^{-3}$ M, $\kappa = 40\,d^{-2}$, $\theta^+_{90,30} = 0.1$, γ in the range $5\,{\rm s}/d^2 \geqslant \gamma \geqslant 5\times10^{-10}\,{\rm s}/d^2$ (from bottom to top).

For the F_1-ATPase model, the numerical analysis in the $f_{\rm ex}\to\infty$ limit yields a linear dependence of $\langle y\rangle$ and j^α_{ij} on $f_{\rm ex}$. We also find that P_2 decays exponentially while P_1 approaches 1. Hence, Ω^{90}_{12} and Ω^{30}_{21} decay exponentially with slope $-d^{90}_{12} = -0.75d$ and $-d^{30}_{21} = -0.25d$, respectively, like in the one-state model but Ω^{90}_{21} now grows exponentially with a smaller exponent while Ω^{30}_{12} still grows linearly.

2. *Without external force*

Just as for the one-state model, we examine the dependence of the coarse-grained rates on the ATP concentration in the absence of external forces.

Figure 10 shows the coarse-grained rates for the 90° and the 30° substeps as well as the average velocity. With decreasing γ, the coarse-grained rates approach the mass action law kinetics for the corresponding one-particle rates. In contrast to the one-state model, even in this limit, the velocity shows saturation. This is due to the fact that the time scale of the hydrolysis reaction is independent of the ATP concentration and represents the limiting effect for the velocity. The dependence of the average velocity on the ATP concentration is reminiscent of a Michaelis-Menten kinetics and coincides well with experimental results for several different probe particles as shown in Ref. [53].

For large beads, the coarse-graining process yields rates that are no longer linear in the corresponding concentrations. In this regime, the sublinear dependence of the velocity on the ATP concentration appears already for smaller ATP concentrations. Comparing the velocity curves of the two-state model with the one-state model, we find that for large beads the velocity curves almost coincide since in this regime the limiting effect for the velocity is the friction experienced by the bead. Thus, using large probe particles, it is not possible to infer the underlying motor dynamics from the characteristics of the velocity as a function of the ATP concentration [25].

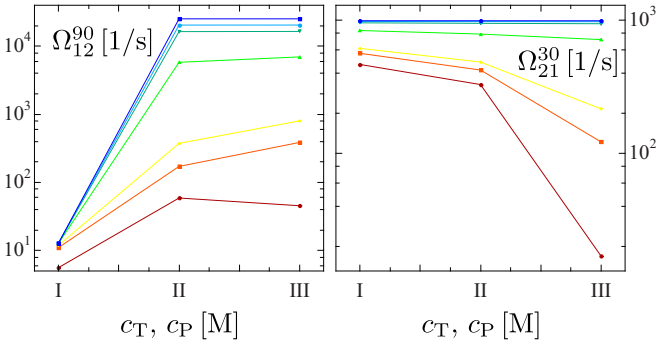

FIG. 11. (Color online) Coarse-grained forward rates for various $\gamma = 2.1\ \mathrm{s}/d^2$, $0.26\ \mathrm{s}/d^2$, $0.14\ \mathrm{s}/d^2$, $0.017\ \mathrm{s}/d^2$, $0.003\ \mathrm{s}/d^2$, $0.001\ \mathrm{s}/d^2$, $3.8 \times 10^{-4}\ \mathrm{s}/d^2$ (from bottom to top) for the parameter sets I: $c_T = 430$ nM, $c_P = 1$ nM; II: $c_T = 1$ mM, $c_P = 1$ nM; III: $c_T = 1$ mM, $c_P = 200$ mM as used in [52]. Parameters that are the same for all sets I–III: $c_D = 1$ nM, $\kappa = 40\ d^{-2}$, $\theta^+_{90,30} = 0.1$ and the attempt frequencies k^α_{ij} as given in Fig. 9. The values of $c_D = c_P = 1$ nM are a rough estimate because there is no information about these concentrations in Ref. [52].

Figure 11 shows the coarse-grained forward rates for three different nucleotide concentrations and for various γ chosen as in the experiment [52]. We find that the 90° rate depends only weakly on γ for small ATP concentrations which is reminiscent of the experimental observation that the ATP binding rate to the motor depends only weakly on the size of the probe [52]. However, for large ATP concentrations that were not investigated in the experiment, the 90° rate shows a strong dependence on γ. This is due to the fact that for small ATP concentrations the relaxation times of all probe particles are in the order of, or even faster than, the motor jump rates. The results for the 30° rate are consistent with experimental results for the hydrolysis rate [52]. Increasing c_P decreases the P_i release rate in the experiment as it decreases the 30° rate here.

D. Example: Kinesin

As a final more complex example, we apply our coarse-graining method to a model with a multistate motor. We choose the well-studied six-state-model representing a kinesin motor introduced in Ref. [5], see Fig. 12. Implementing the probe particle and an elastic linker $V(y)$, we adopt the transition rates of the motor from [5] and replace the dependence on the external force by the dependence on the elongation of the linker,

$$w^+_{25}(y) = k_{25} \exp[-V(y + d\theta^+) + V(y)], \tag{39}$$

$$w^-_{52}(y) = k_{52} \exp[-V(y - d\theta^-) + V(y)], \tag{40}$$

$$w^+_{ij,\mathrm{chem}} = k_{ij} \frac{2 \exp[\mu^+_{ij}]}{1 + \exp[\partial_y V(y) \chi_{ij}]}, \tag{41}$$

$$w^-_{ji,\mathrm{chem}} = k_{ji} \frac{2 \exp[\mu^-_{ij}]}{1 + \exp[\partial_y V(y) \chi_{ij}]}. \tag{42}$$

The first two rates belong to the mechanical transition, the lower two rates represent the chemical transitions which depend on the instantaneous force exerted by the linker with a chemical load-sharing factor χ_{ij}, see Ref. [5]. The change

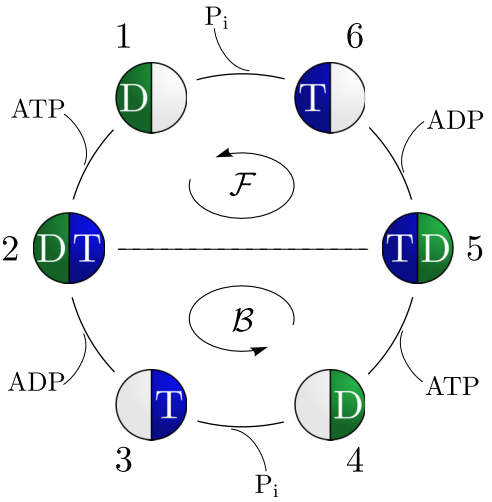

FIG. 12. (Color online) Six-state-model representing a kinesin motor adapted from Ref. [5]. The transition between states 2 and 5 is purely mechanical and corresponds to a step of length d whereas all other transitions are pure chemical transitions. The motor model includes three cycles: $\mathcal{F}$, which, in the + direction, includes ATP hydrolysis and forward stepping; $\mathcal{B}$, which includes ATP hydrolysis and backward stepping in its + direction; and a pure chemical cycle (around the circle) that includes hydrolysis or synthesis of two ATP.

of chemical free energy $\mu^\pm_{ij} = \mu_T, \mu_D, \mu_P$ depends on which transition involves binding of the corresponding nucleotide. We choose again $V(y) = \kappa y^2/2$.

The coarse-grained rates for the mechanical transition are shown in Fig. 13. With decreasing γ, the rates approach their fast-bead limit which corresponds to the rates used in Ref. [5] while strong deviations occur for finite γ especially for assisting external forces. The friction coefficient of a probe of size 500 nm as in Ref. [55] can be calculated using Stokes's law yielding $\gamma \simeq 7.7 \times 10^{-5}\ d^2/\mathrm{s}$. For friction coefficients in this range [light green (light gray) line with triangles],

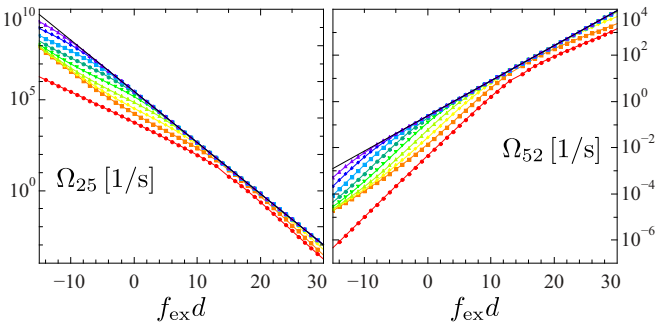

FIG. 13. (Color online) Coarse-grained rates for the mechanical transitions (with y dependence) for various γ in the range $0.077\ \mathrm{s}/d^2 \geqslant \gamma \geqslant 7.7 \times 10^{-10}\ \mathrm{s}/d^2$ (from bottom to top). The rates approach the one-particle rates from Ref. [5] (solid black lines). Parameters: $\kappa = 10\ d^{-2}$ [55], $c_T = 0.001$ M, $c_D = c_P = 10^{-9}$ M (estimated), $\theta^+ = 0.65$, $\chi_{ij} = 0.25, 0.15$, $k_{12} \exp[\mu^{\mathrm{eq}}_T]/c^{\mathrm{eq}}_T = k_{45} \exp[\mu^{\mathrm{eq}}_T]/c^{\mathrm{eq}}_T = 2 \times 10^6\ (\mathrm{Ms})^{-1}$, $k_{21} = k_{23} = k_{34} = k_{56} = k_{61} = 100\ (\mathrm{s})^{-1}$, $k_{32} \exp[\mu^{\mathrm{eq}}_D]/c^{\mathrm{eq}}_D = k_{65} \exp[\mu^{\mathrm{eq}}_D]/c^{\mathrm{eq}}_D = 2 \times 10^4\ (\mathrm{Ms})^{-1}$, $k_{43} \exp[\mu^{\mathrm{eq}}_P]/c^{\mathrm{eq}}_P = k_{16} \exp[\mu^{\mathrm{eq}}_P]/c^{\mathrm{eq}}_P = 2 \times 10^4\ (\mathrm{Ms})^{-1}$, $k_{25} = 3 \times 10^5\ (\mathrm{s})^{-1}$, $k_{52} = 0.24\ (\mathrm{s})^{-1}$, $k_{54} = (k_{52}/k_{25})^2 k_{21}$.

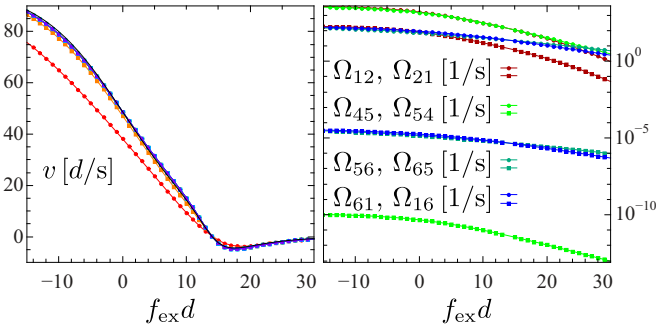

FIG. 14. (Color online) Left: Average velocity for the model with probe particle (colored lines with symbols) an the one-particle model from Ref. [5] (solid black line). Right: Coarse-grained rates for chemical transitions (with y dependence) for $\gamma = 0.077\ \mathrm{s}/d^2$. Other parameters as given in Fig. 13.

our coarse-grained rates show a distinct deviation from the one-particle rates (solid black lines). However, the average velocity (obtained from our coarse-grained rates) as function of the external force coincides very well for almost all γ with the velocity curve obtained from the bare motor model, see Fig. 14. Like for the F_1-ATPase model discussed in Sec. III C, this agreement is due to the fact that the velocity involves only the difference of the rates multiplied with the marginal distribution. If one investigates only force-velocity curves, the discrepancies between the coarse-grained rates and the one-particle rates are hardly visible.

In contrast to the coarse-grained rates of the F_1-ATPase models, the coarse-grained rates for the mechanical transition of the kinesin model show more structure especially for negative, i.e., assisting external forces. Since the kinesin model contains several internal motor cycles, depending on the external force the dominant cycle can change, leading to crossover regimes with changing weight of the probabilities P_i.

The dependence of the coarse-grained rates for chemical transitions on the external force is visible in Fig. 14. Although there is no explicit dependence on external forces for pure chemical rates since $d_{ij}^{\alpha} = 0$, j_{ij}^{α} and P_i depend on f_{ex} via y. The operational current for transitions within the $\mathcal{F}$ cycle in + direction decreases with increasing f_{ex}, whereas the operational currents within the $\mathcal{B}$ cycle in + direction slightly increase with f_{ex}, which can be explained intuitively since the motor prefers "backward" cycles for large opposing forces. However, all coarse-grained rates decrease with increasing f_{ex}, similarly to the bare motor rates (41) and (42) which decrease with larger y, a situation that is more likely to appear for large external forces.

IV. EXPERIMENTAL IMPLEMENTATION

In order to practically apply the coarse-grained description, one has to determine the marginal distributions P_i, the operational currents j_{ij}^{α}, and the free-energy differences ΔF_{ij}^{α}. For multistate motors, this is a rather challenging task since only a few quantities can be extracted reliably from the experimentally measured trajectory of the probe. Note, however, that this problem does not happen exclusively in our approach but is inevitable whatever method is used to infer motor properties from such trajectories.

In the following, using the 90-30 model for the F_1-ATPase, we will illustrate how these quantities can be estimated. If all motor transitions involve mechanical transitions with different step sizes, the plateaus in the probe trajectory can be assigned to specific corresponding motor states. Since after a large-enough time interval all possible transitions will have occurred, one is also able to reconstruct the links connecting the states. The marginal distributions P_i are then given as the fraction of time that the corresponding motor state is occupied. For the two-state model of the F_1-ATPase, we assign plateaus in the probe trajectory that are followed by a fast 90° forward or 30° backward displacement to motor state $i = 1$ and plateaus that are followed by fast 90° backward or 30° forward displacement to $i = 2$. In principle, there are several possibilities to reconstruct hidden variables from partially visible trajectories [59–61]. Here we will use a simple algorithm which sets $i = 2$ if four consecutive data points are within a specific range around 90° and otherwise $i = 1$. The marginal distributions P_1, P_2 are then represented by the fraction of data points with assigned $i = 1,2$.

If the motor is not very complex, the operational currents j_{ij}^{α} can be obtained rather easily since they are precisely the net currents between two motor states. For unicyclic motors, all operational currents are equal to the average velocity divided by d, the operational current of an ATP binding transition is the net disappearance rate of ATP in the solution (given that there are no other ATP binding reactions), and so on. If all motor transitions involve mechanical transitions with different step sizes, the operational currents between any two states can be obtained by counting the number of transitions of a specific step size from $i \to j$, n_{ij}^{α}, and $j \to i$, n_{ji}^{α}. The (time) average of this current using one long trajectory of length t_{tot} is then given by

$$j_{ij}^{\alpha} = \left(n_{ij}^{\alpha} - n_{ji}^{\alpha}\right)/t_{\mathrm{tot}}. \tag{43}$$

In our example, in order to estimate j_{12}^{90} we have to count the number of sudden displacements of "size" 90° either from the trajectory of the probe directly or from the reconstructed trajectory of the motor using the assignment rule mentioned above. If the time resolution of the trajectory is very coarse or if the reconstruction method is rather inaccurate, jumps that consist of fast consecutive 90 and 30 jumps with apparent step size 120° will appear which have to be included in the number of 90° (and also 30°) jumps. Figure 15 shows a reconstructed motor trajectory obtained with the algorithm mentioned above. We have used a trajectory of the probe from our simulations as "experimental data." Compared to the original motor trajectory, this reconstruction captures the average dynamics quite well. Large fluctuations of the probe can generate additional apparent motor jumps in the reconstructed trajectory that are absent in the original one.

Finally, the estimation of the free-energy difference $\Delta F_{ij}^{\alpha} = F_j - F_i - \Delta\mu_{ij}^{\alpha}$ is slightly more involved. In equilibrium ($\Delta\mu = 0$, $f_{\mathrm{ex}} = 0$), detailed balance holds,

$$\frac{w_{ij}^{\alpha}(y)}{w_{ji}^{\alpha}\left(y + d_{ij}^{\alpha}\right)} = \frac{p_j^{\mathrm{eq}}\left(y + d_{ij}^{\alpha}\right)}{p_i^{\mathrm{eq}}(y)}, \tag{44}$$

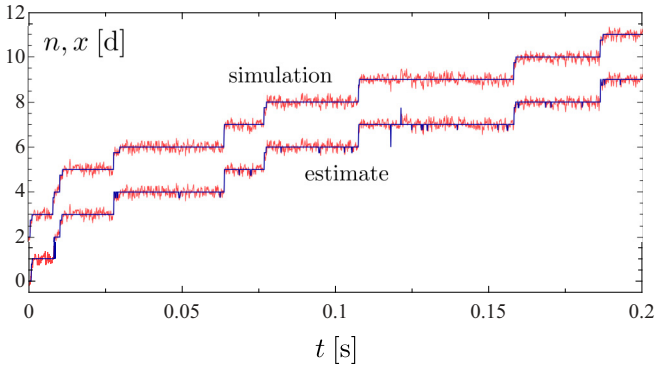

FIG. 15. (Color online) Comparison of the simulated trajectory of motor and probe with a trajectory of the probe and the estimated motor position that was reconstructed using the simulated trajectory of the probe. The trajectories are shifted for better visibility. Parameters: $\kappa = 40\, d^{-2}$, $\gamma = 0.005\ \mathrm{s}/d^2$, $c_T = c_D = 2 \times 10^{-6}$ M, $c_P = 10^{-3}$ M, $c_T^{\mathrm{eq}} = 3.33 \times 10^{-7}$ M, $c_D^{\mathrm{eq}} = 0.0682$ M, $c_P^{\mathrm{eq}} = 1$ M, $f_{\mathrm{ex}} = 0$, lower boundary to set $i = 2$: $x - \lfloor x \rfloor = 0.375d$, upper boundary to set $i = 2$: $x - \lfloor x \rfloor = 0.89d$.

with the Boltzmann distribution $p_i^{\mathrm{eq}}(y) = P_i^{\mathrm{eq}} \exp[-V(y)]/\mathcal{N}$. Inserting this expression yields

$$P_j^{\mathrm{eq}} / P_i^{\mathrm{eq}} = \exp\left[-F_j + F_i + \Delta\mu_{ij}^{\alpha,\mathrm{eq}}\right] \equiv \exp\left[-\Delta\mathcal{F}_{ij}^{\alpha}\right] \quad (45)$$

for the marginal distributions in equilibrium. Note that $\Delta\mu_{ij}^{\alpha,\mathrm{eq}} \neq 0$ if the corresponding transition comprises only binding or release of nucleotides. Thus, the equilibrium free-energy difference $\Delta\mathcal{F}_{ij}^{\alpha}$ (which explicitly depends on the equilibrium concentrations) can be obtained from the ratio of the marginal distributions under equilibrium conditions. Using $\mu_i = \mu_i^{\mathrm{eq}} + \ln(c_i/c_i^{\mathrm{eq}})$, we find that

$$\Delta F_{ij}^{\alpha} = \Delta\mathcal{F}_{ij}^{\alpha} \pm \sum_k \ln \frac{c_k}{c_k^{\mathrm{eq}}} \quad (46)$$

with $k = T, D, P$ and the sign depending on which binding or release event corresponds to the transition ij,α [62]. Hence, the free-energy difference ΔF_{ij}^{α} needed for the coarse-grained rates can be expressed by the equilibrium free-energy difference $\Delta\mathcal{F}_{ij}^{\alpha}$ obtained from experimental data at equilibrium conditions and the nucleotide concentrations with respect to the equilibrium concentrations corresponding to the conditions used to obtain $\Delta\mathcal{F}_{ij}^{\alpha}$. For the 90-30 model, we have $P_2^{\mathrm{eq}}/P_1^{\mathrm{eq}} = \exp[-\Delta\mathcal{F}_{12}^{90}] = \exp[-\Delta\mathcal{F}_{12}^{30}]$ with $-\Delta\mathcal{F}_{12}^{90} = -F_2 + F_1 + \mu_T^{\mathrm{eq}} - \mu_D^{\mathrm{eq}} = -F_2 + F_1 + \mu_P^{\mathrm{eq}} = -\Delta\mathcal{F}_{12}^{30}$ since $\Delta\mu = 0$ in equilibrium.

Once these quantities have been estimated, there are no additional fit parameters needed or left. All concentrations as well as the external force are usually known from the experimental setup. To obtain the coarse-grained rates from the probe trajectory of our 90-30 model, we then proceed as follows. First, we choose equilibrium conditions and obtain $\Delta\mathcal{F}_{12}$ from the ratio of marginal distributions. Then we change to nonequilibrium concentrations and estimate P_1, P_2 and the operational current j_{12}^{90}. The coarse-grained rates, according to Eqs. (24) and (25), are then given by

TABLE I. Comparison of the coarse-grained rates and other relevant quantities obtained from the simulation of the full model with the ones estimated using the reconstructed motor trajectory. The trajectory used to obtain these values is shown in Fig. 15.

	Simulation	Estimate
P_1	0.944	0.952
P_2	0.056	0.048
j_{12}^{90} (1/s)	52.292	52.246
$\Delta\mathcal{F}_{12}$	3.216	3.140
Ω_{12}^{90} (1/s)	55.325	54.899
Ω_{21}^{90} (1/s)	0.006 76	0.006 20
Ω_{21}^{30} (1/s)	937.1	1082.37
Ω_{12}^{30} (1/s)	0.037	0.046

$$\Omega_{12}^{90} = j_{12}^{90} \frac{c_T c_D^{\mathrm{eq}} \exp\left[-\Delta\mathcal{F}_{12} - f_{\mathrm{ex}} d_{12}^{90}\right]/\left(c_T^{\mathrm{eq}} c_D\right)}{P_1 c_T c_D^{\mathrm{eq}} \exp\left[-\Delta\mathcal{F}_{12} - f_{\mathrm{ex}} d_{12}^{90}\right]/\left(c_T^{\mathrm{eq}} c_D\right) - P_2}, \quad (47)$$

$$\Omega_{21}^{90} = j_{12}^{90} \frac{1}{P_1 c_T c_D^{\mathrm{eq}} \exp\left[-\Delta\mathcal{F}_{12} - f_{\mathrm{ex}} d_{12}^{90}\right]/\left(c_T^{\mathrm{eq}} c_D\right) - P_2}, \quad (48)$$

$$\Omega_{21}^{30} = j_{12}^{90} \frac{c_P^{\mathrm{eq}} \exp\left[\Delta\mathcal{F}_{12} - f_{\mathrm{ex}} d_{21}^{30}\right]/c_P}{P_2 c_P^{\mathrm{eq}} \exp\left[\Delta\mathcal{F}_{12} - f_{\mathrm{ex}} d_{21}^{30}\right]/c_P - P_1}, \quad (49)$$

$$\Omega_{12}^{30} = j_{12}^{90} \frac{1}{P_2 c_P^{\mathrm{eq}} \exp\left[\Delta\mathcal{F}_{12} - f_{\mathrm{ex}} d_{21}^{30}\right]/c_P - P_1}. \quad (50)$$

A comparison of the coarse-grained rates and related quantities obtained from the full theoretical model and from the reconstructed one estimated using the probe trajectory is shown in Table I. We find quite good agreement between the original and the reconstructed quantities with a maximum error of 14% except for the Ω_{ij}^{30} rates which have a maximum error of 24%.

The 90-30 model thus provides a useful demonstration of the experimental applicability of the coarse-graining method showing that it is possible to estimate the coarse-grained rates from experimental accessible data if the underlying motor network is not too complex. Considering the simplicity of the applied reconstruction method, the accuracy of the estimates is rather encouraging.

V. INVARIANCE OF ENTROPY PRODUCTION AND EFFICIENCY

An important question for any coarse-graining method concerns its effect on entropy production. In general, a coarse-grained description without imposed time-scale separation or detailed balance for the eliminated variables often underestimates the entropy production of the system [29–32,40]. In this section, we show that for the type of models considered here, our coarse-graining method conserves the entropy production even if there is no time-scale separation between the eliminated and remaining degree of freedom.

Since transitions can be uniquely attributed to motor or probe particle, the total entropy production of the system [28] can be split in two parts, analogously to bipartite or partially masked systems [63,64],

$$\begin{aligned}\dot{S}_{\rm tot} &= \sum_i \int_{-\infty}^{\infty} \frac{\gamma j_i^{x\,2}(y)}{p_i(y)} dy \\ &\quad + \sum_{i,j,\alpha} \int_{-\infty}^{\infty} p_i(y) w_{ij}^{\alpha}(y) \ln \frac{p_i(y) w_{ij}^{\alpha}(y)}{p_j\big(y + d_{ij}^{\alpha}\big) w_{ji}^{\alpha}\big(y + d_{ij}^{\alpha}\big)} dy \\ &\equiv \dot{S}_{\rm tot}^{\rm p} + \dot{S}_{\rm tot}^{\rm m}, \end{aligned} \tag{51}$$

where $j_i^x(y) = \{[\partial_y V(y) - f_{\rm ex}] p_i(y) + \partial_y p_i(y)\}/\gamma$ is the current due to the motion of only the bead for fixed i. Obviously, both $\dot{S}_{\rm tot}^{\rm p}$ and $\dot{S}_{\rm tot}^{\rm m}$ are non-negative.

The total entropy production (51) can be calculated using the LDB condition (19) as

$$\begin{aligned}\dot{S}_{\rm tot} &= \sum_i \int_{-\infty}^{\infty} [\partial_y V(y) - f_{\rm ex}] j_i^x(y) dy \\ &\quad + \sum_{i,j,\alpha} \int_{-\infty}^{\infty} p_i(y) w_{ij}^{\alpha}(y) \big[\Delta\mu_{ij}^{\alpha} - F_j + F_i \\ &\quad - V\big(y + d_{ij}^{\alpha}\big) + V(y)\big] dy \\ &= \sum_{i<j,\alpha} \Delta\mu_{ij}^{\alpha} j_{ij}^{\alpha} - f_{\rm ex} v \geqslant 0. \end{aligned} \tag{52}$$

Using partial integration, it can be easily seen that the parts involving $V(y)$ cancel, i.e., the energy of the linker is constant on average. The total entropy production is then given by the chemical free-energy consumption that is not transformed into mechanical power.

For the coarse-grained description, the total entropy production contains only contributions from the effective jump process,

$$\dot{S}_{\rm tot}^{\rm cg} = \sum_{i,j,\alpha} P_i \Omega_{ij}^{\alpha} \ln \frac{P_i \Omega_{ij}^{\alpha}}{P_j \Omega_{ji}^{\alpha}} = \sum_{i,j,\alpha} P_i \Omega_{ij}^{\alpha} \ln \frac{\Omega_{ij}^{\alpha}}{\Omega_{ji}^{\alpha}}. \tag{53}$$

Using the LDB condition for the coarse-grained rates (20) and the condition on the operational current (21) yields

$$\dot{S}_{\rm tot}^{\rm cg} = \sum_{i<j,\alpha} \Delta\mu_{ij}^{\alpha} j_{ij}^{\alpha} - f_{\rm ex} v, \tag{54}$$

which is precisely (52). For these models for which the state space of the eliminated degree of freedom does not contain entropy producing internal cycles, the average total entropy production in the NESS remains invariant under our coarse-graining procedure.

It is also instructive to apply the entropy-splitting scheme introduced in Ref. [31] to our coarse-graining procedure. In Ref. [31], it was shown that the total entropy production can be written as a sum of the coarse-grained entropy production (53) plus a contribution of the microstates corresponding to a mesostate (which are eliminated during coarse-graining) plus a contribution due to the fact that jumps between mesostates can occur involving different microstates. In our framework, the total entropy production is already recovered by the coarse-grained entropy production. The two additional contributions which correspond to the total entropy production of the probe particle and the average total entropy production of the motor minus the coarse-grained entropy production cancel each other.

We finally show that our coarse-graining procedure also preserves the energy transduction, or thermodynamic, efficiency η_T defined as the ratio of the extractable power $\dot{W}_{\rm out}$ and the rate of chemical energy input $\dot{\Delta\mu}$ [65],

$$\eta_T \equiv \frac{\dot{W}_{\rm out}}{\dot{\Delta\mu}}. \tag{55}$$

For the systems we have studied so far, as long as the external force is smaller than the stall force, the power output is given by $\dot{W}_{\rm out} = f_{\rm ex} v$ and the power input by $\sum_{i<j,\alpha} \Delta\mu_{ij}^{\alpha} j_{ij}^{\alpha}$, which leads to the efficiency

$$\eta_T = \frac{f_{\rm ex} v}{\sum_{i<j,\alpha} \Delta\mu_{ij}^{\alpha} j_{ij}^{\alpha}}, \tag{56}$$

which is the same in the coarse-grained description since v, j_{ij}^{α}, and $\Delta\mu_{ij}^{\alpha}$ are conserved.

For motor models with tight coupling or multistate models with a single motor cycle, the rate of chemical energy input equals the velocity $\dot{\Delta\mu} = v\Delta\mu/d$ and the efficiency reduces to $\eta_T = f_{\rm ex}/\Delta\mu$. In general, however, any idle cycles of the motor increases the rate of chemical input over the velocity and therefore reduces the efficiency.

VI. STALL FORCE AND RATE ANOMALY

Coarse-graining multicyclic motor models as developed here reveals a remarkable feature concerning the stall force with significant implications on the interpretation of experimental data. For an example, consider the kinesin motor for the parameters chosen in Fig. 13. Figure 16 shows that the stall force is a function of the size of the attached probe particle. Generally speaking, the stall force can indeed depend on the size of the probe since the network of the full system comprises more cycles than the coarse-grained or bare motor network, see Fig. 7. Varying the size of the probe, the relative weight of the cycles in the full system and hence their contribution to an operational current can change yielding a varying stall force. Thus, the experimentally obtained stall force corresponds to

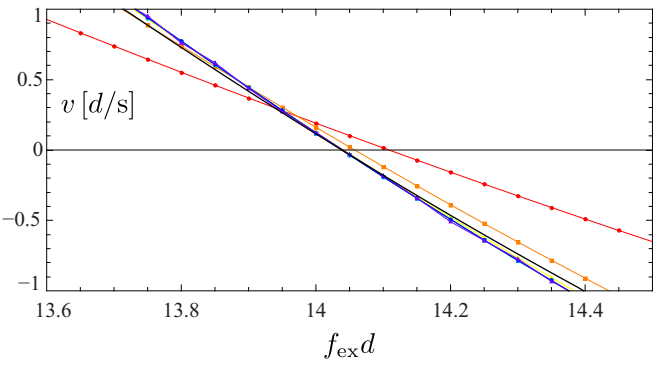

FIG. 16. (Color online) Average velocity of the kinesin model as a function of the external force. Depending on the size of the probe, stall conditions are reached for different values of the external force. Parameters as in Fig. 13.

the stall conditions of the motor-probe complex but does not necessarily represent the stall conditions of the bare motor. If one is interested in the latter one should use very small probe particles since the limit of vanishing friction coefficient γ is equivalent to applying the force directly to the motor. As discussed below, the stall force is independent of γ for one-state or unicyclic multistate motor models. Hence, an experimentally observed variation of the stall force with probe size can be used as proof that the motor is indeed multicyclic.

The varying stall force has also implications on the transition rates. In Fig. 13, a close look around $f_{\mathrm{ex}}d = 14$ shows that these data points are missing for the following reason. For all investigated models, we find that if, as a function of the external force, the sign change of an operational current depends on the friction coefficient γ, the coarse-grained rates corresponding to this transitions can become piecewise negative. This phenomenon occurs when the affinity of the affected transitions, $\ln[P_i\Omega^{\alpha}_{ij}/(P_j\Omega^{\alpha}_{ji})]$, has the opposite sign of j^{α}_{ij}. An isolated sign change in the denominator of Eqs. (24) and (25) leads to a pole in the corresponding rate. Such an anomaly in Ω^{α}_{ij} necessarily implies a corresponding one in Ω^{α}_{ji} since the ratio of the effective rates obeys the local detailed balance condition which enforces the same sign for both rates. In this range, the coarse-graining scheme introduced here fails to produce physically acceptable rates. In practice, one should discard the results at least when either a rate is negative or becomes larger than the rate for vanishing bead size. In Fig. 17, where we zoom into the range around the stall force, this range is shaded gray. Taken at face value, this phenomenon looks like a shortcoming of our approach. It is the price to pay for requiring over the full parameter range both the local detailed balance condition and the correct net currents from any one motor state to any other. While the negative rates do not allow for a sensible physical interpretation, they nevertheless can be used to calculate average quantities and yield, e.g., the correct entropy production as shown in Sec. V.

This stall force anomaly with a corresponding range of negative rates occurs neither for any one-state motor model nor for unicyclic motors around stall conditions since only one motor cycle contributes to all cycles of the full system causing the zero of j^{α}_{ij} and $\ln[P_i\Omega^{\alpha}_{ij}/(P_j\Omega^{\alpha}_{ji})]$ to occur for the same f_{ex}. We also found several multicyclic motors that do not lead to negative rates, e.g., the kinesin model if one assumes

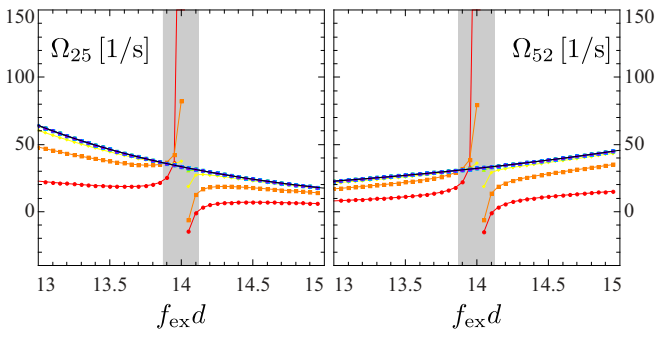

FIG. 17. (Color online) Detail of the coarse-grained mechanical transition rates of the kinesin model as shown in Fig. 13. Near the stall force at $f_{\mathrm{ex}}d \simeq 14$ these rates exhibit a pole. In the gray shaded range, they should not be interpreted as physical transition rates.

the chemical rates to be independent of y. A derivation of the precise conditions under which for multistate motor models a pair of effective rates diverges or becomes negative must be left to future work. We stress, however, that in all examples shown in this study, this anomaly occurs only in the narrow range shown in Fig. 17. From a practical point of view, it therefore may not be as relevant as it is intriguing from a theoretical perspective.

VII. CONCLUSION

Most experiments on molecular motors comprise some kind of probe particle. Therefore, any theoretical modeling with parameters estimated from experimental data will explicitly or implicitly contain characteristics of the probe particle.

In this paper, we have introduced a systematic coarse-graining method that allows us to reduce motor-bead models to effective one-particle motor models. This coarse-graining procedure provides a compromise between a one-particle description that is simple to handle and a detailed model comprising the dynamics of the full system. It yields an effective one-particle model maintaining the true motor network, where the influence of the probe is naturally incorporated without any additional assumptions since the simplification of the description takes place *a posteriori*. Any external force acting on the probe is then acting on the effective motor directly. The coarse-grained rates obey a LDB condition and yield the correct net currents. Fixing the marginal distribution and the average currents, there is still freedom on how to choose the rates. Only with the LDB condition the effective rates are determined uniquely.

Applying the coarse-graining procedure to motor-bead models, we find that in general the coarse-grained rates do not show a single exponential dependence on the external force in contrast to what is often assumed for mechanical transition rates in one-particle models. Only in the often unrealistic limit of fast bead relaxation, the coarse-grained rates reduce to the corresponding one-particle rates.

In the absence of external forces, in general the coarse-grained rates are not proportional to the ATP concentration even if the motor rates obey mass action law kinetics. This feature originates from the drag effect of probe (due to friction) that is incorporated in the coarse-grained rates. For the same reason, the average velocity shows a sublinear dependence on the ATP concentration even for a one-state motor model. Assuming an *a priori* one-particle model with external force acting directly on the motor, one would have either to use a rather counterintuitive complex force-dependence of the transition rates or to introduce additional motor states in order to obtain a sublinearly growing velocity caused by the drag of the probe. In a one-particle description, the effect of large probe particles on the dwell time distributions could also be mistaken as signature of additional motor states, thus leading to an overly complex motor network [21,56].

Considering the influence of the coarse-graining procedure on the stochastic thermodynamics of the system, we show that the total entropy production remains invariant under coarse-graining. This is due to the fact that, on the one hand, the state space of the eliminated degree of freedom contains no entropy producing cycles. On the other hand the design

of the coarse-graining procedure is also important. It has to conserve the motor network as well as the net currents and provide transition rates that fulfill a LDB condition. Likewise, the thermodynamic efficiency remains invariant in our scheme.

Our coarse-graining method conserves average quantities like the entropy production or operational currents although eliminating the dynamics of the probe particle strongly affects the cycle structure of the full system. In order to preserve also fluctuations of current observables in the long-time limit it was found that coarse-graining methods should conserve the cycle structure of the full system [36,37].

From the experimental point of view, in order to obtain the simpler effective model, the underlying mesoscopic modeling need not to be known since all these quantities enter the coarse-grained description via the net currents and the marginal distributions which, in principle, can be extracted from the experimental data as we have demonstrated using a two-step model for the F_1-ATPase.

The main advantage of the coarse-graining procedure introduced here is that once the rates have been obtained from experimentally accessible quantities, they automatically fulfill a LDB condition and provide the correct average currents, i.e., velocity, entropy production, hydrolysis rate, and so on.

For multicyclic motors, the coarse-graining procedure can yield rates that can have poles and become (piecewise) negative. If this scenario occurs, the coarse-grained rates lack a physical interpretation as transition probabilities in this range but they can still be used to calculate average quantities. For this class of motors the stall force typically depends on the size of the probe particle, i.e., the friction coefficient. Applying naively a one-particle model to such an experimental setup would not allow us to determine the energy transduction mechanism of the motor correctly. For one-state motors, the coarse-grained rates are always positive.

So far, we have discussed coarse-graining only under NESS conditions. In principle, the coarse-graining procedure as introduced in Secs. II B and III A can also be applied to non-stationary states, e.g., if the nucleotide concentrations are not constant and $\Delta\mu$ decreases with time [62,66]. Such a scenario would yield time-dependent P_i's, net currents, LDB conditions, and therefore also time-dependent coarse-grained rates.

Further generalizations might include other types of models representing the full system. While developed here for discrete motor models, the coarse-graining procedure should be also applicable to continuous motors moving in a tilted periodic potential where the potential minima will become the discrete states of the coarse-grained effective motor. The introduction of the index α in principle also accounts for more involved potentials or free-energy surfaces that depend on both the motor and the probe state.

ACKNOWLEDGMENTS

E.Z. thanks P. Pietzonka for valuable hints concerning numerical implementations.

APPENDIX: LIMITING CASE: LARGE APPLIED FORCE

In the limit of large external forces, $f_{\mathrm{ex}} \to \infty$, the coarse-grained rates (7) and (8) can be expressed as

$$\Omega^+ \approx -v \exp[\Delta\mu - f_{\mathrm{ex}} d]/d, \tag{A1}$$

$$\Omega^- \approx -v/d. \tag{A2}$$

While $\Delta\mu$ is independent of the external force, the average velocity is a function of the external force,

$$v = \langle \partial_y V(y) - f_{\mathrm{ex}} \rangle / \gamma = \kappa \langle y \rangle / \gamma - f_{\mathrm{ex}}/\gamma. \tag{A3}$$

It becomes negative for forces larger than the stall force $\Delta\mu/d$, which ensures that both Ω^+ and Ω^- are positive. If there is no time-scale separation between the dynamics of motor and probe, $\langle y \rangle$ grows linearly in f_{ex} for $f_{\mathrm{ex}} \to \infty$ with a smaller slope than $1/\kappa$. On the other hand, with time-scale separation, we have $\langle y \rangle = f_{\mathrm{ex}}/\kappa$. Note that within time-scale separation, the average velocity has to be calculated using the average velocity of the motor, Eq. (4), since the "average velocity" of the probe $\langle \partial_y V(y) - f_{\mathrm{ex}} \rangle / \gamma$ is zero as a result of the fast-bead limit of Eq. (3). Due to the linear dependence of $\langle y \rangle$ on f_{ex}, the average velocity, and therefore also Ω^-, are then proportional to the external force, whereas the exponential factor dominates for Ω^+,

$$\Omega^+ \sim f_{\mathrm{ex}} \exp[\Delta\mu - f_{\mathrm{ex}} d]/(\gamma d), \tag{A4}$$

$$\Omega^- \sim f_{\mathrm{ex}}/(\gamma d). \tag{A5}$$

In the opposite limit of a large assisting force $f_{\mathrm{ex}} \to -\infty$, the coarse-grained rates (7) and (8) become

$$\Omega^+ \approx v/d, \tag{A6}$$

$$\Omega^- \approx v \exp[-\Delta\mu + f_{\mathrm{ex}} d]/d. \tag{A7}$$

As above, the average y grows linearly and the velocity is proportional to f_{ex} if there is no time-scale separation which leads to

$$\Omega^+ \sim |f_{\mathrm{ex}}|/(\gamma d), \tag{A8}$$

$$\Omega^- \sim |f_{\mathrm{ex}}| \exp[-\Delta\mu + f_{\mathrm{ex}} d]/(\gamma d). \tag{A9}$$

This simple analysis clearly shows that the coarse-grained rates do not coincide with the often *a priori* assumed single exponential force dependence of one-particle rates. Within our numerical analysis, the asymptotic behavior appears for $|f_{\mathrm{ex}}| \gtrsim 500/d$. The regime for large forces shown in Figs. 2 and 3 is not the asymptotics yet. However, since $\langle y \rangle$ is also linear in f_{ex} in this region yet with different slope, v is still proportional to f_{ex}.

[1] A. B. Kolomeisky, Motor proteins and molecular motors: How to operate machines at the nanoscale, J. Phys.: Condens. Matter **25**, 463101 (2013).

[2] D. Chowdhury, Stochastic mechano-chemical kinetics of molecular motors: A multidisciplinary enterprise from a physicist's perspective, Phys. Rep. **529**, 1 (2013).

[3] A. B. Kolomeisky and M. E. Fisher, Molecular motors: A theorist's perspective, Ann. Rev. Phys. Chem. **58**, 675 (2007).

[4] A. W. C. Lau, D. Lacoste, and K. Mallick, Non-equilibrium fluctuations and mechanochemical couplings of a molecular motor, Phys. Rev. Lett. **99**, 158102 (2007).

[5] S. Liepelt and R. Lipowsky, Kinesin's network of chemomechanical motor cycles, Phys. Rev. Lett. **98**, 258102 (2007).

[6] R. Lipowsky and S. Liepelt, Chemomechanical coupling of molecular motors: Thermodynamics, network representations, and balance conditions, J. Stat. Phys. **130**, 39 (2008).

[7] R. Lipowsky, S. Liepelt, and A. Valleriani, Energy conversion by molecular motors coupled to nucleotide hydrolysis, J. Stat. Phys. **135**, 951 (2009).

[8] R. D. Astumian, Thermodynamics and kinetics of molecular motors, Biophys. J. **98**, 2401 (2010).

[9] F. Jülicher, A. Ajdari, and J. Prost, Modeling molecular motors, Rev. Mod. Phys. **69**, 1269 (1997).

[10] P. Reimann, Brownian motors: Noisy transport far from equilibrium, Phys. Rep. **361**, 57 (2002).

[11] M. E. Fisher and A. B. Kolomeisky, The force exerted by a molecular motor, Proc. Natl. Acad. Sci. U.S.A. **96**, 6597 (1999).

[12] H. Qian, A simple theory of motor protein kinetics and energetics. II, Biophys. Chem. **83**, 35 (2000).

[13] Y. C. Kim and M. E. Fisher, Vectorial loading of processive motor proteins: Implementing a landscape picture, J. Phys.: Condens. Matter **17**, S3821 (2005).

[14] S. Liepelt and R. Lipowsky, Steady-state balance conditions for molecular motor cycles and stochastic nonequilibrium processes, Europhys. Lett. **77**, 50002 (2007).

[15] U. Seifert, Efficiency of autonomous soft nano-machines at maximum power, Phys. Rev. Lett. **106**, 020601 (2011).

[16] N. Golubeva and A. Imparato, Efficiency at maximum power of interacting molecular machines, Phys. Rev. Lett. **109**, 190602 (2012).

[17] N. Golubeva and A. Imparato, Maximum power operation of interacting molecular motors, Phys. Rev. E **88**, 012114 (2013).

[18] P. Gaspard and E. Gerritsma, The stochastic chemomechanics of the F1-ATPase molecular motor, J. Theor. Biol. **247**, 672 (2007).

[19] N. Golubeva, A. Imparato, and L. Peliti, Efficiency of molecular machines with continuous phase space, Europhys. Lett. **97**, 60005 (2012).

[20] Y. Chen, Theoretical formalism for kinesin motility I. bead movement powered by single one-headed kinesins, Biophys. J. **78**, 313 (2000).

[21] R. E. L. DeVille and E. Vanden-Eijnden, Regular gaits and optimal velocities for motor proteins, Biophys. J. **95**, 2681 (2008).

[22] A. Kunwar, M. Vershinin, J. Xu, and S. P. Gross, Stepping, strain gating, and an unexpected force-velocity curve for multiple-motor-based transport, Curr. Biol. **18**, 1173 (2008).

[23] C. B. Korn, S. Klumpp, R. Lipowsky, and U. S. Schwarz, Stochastic simulations of cargo transport by processive molecular motors, J. Chem. Phys. **131**, 245107 (2009).

[24] S. Bouzat and F. Falo, The influence of direct motor-motor interaction in models for cargo transport by a single team of motors, Phys. Biol. **7**, 046009 (2010).

[25] S. J. Lade, E. M. Craig, and H. Linke, Effectiveness of beads for tracking small-scale molecular motor dynamics, Phys. Rev. E **84**, 021907 (2011).

[26] E. Zimmermann and U. Seifert, Efficiency of a molecular motor: A generic hybrid model applied to the F1-ATPase, New J. Phys. **14**, 103023 (2012).

[27] P. Pietzonka, E. Zimmermann, and U. Seifert, Fine-structured large deviations and the fluctuation theorem: Molecular motors and beyond, Europhys. Lett. **107**, 20002 (2014).

[28] U. Seifert, Stochastic thermodynamics, fluctuation theorems, and molecular machines, Rep. Prog. Phys. **75**, 126001 (2012).

[29] S. Rahav and C. Jarzynski, Fluctuation relations and coarse-graining, J. Stat. Mech.: Theor. Exp. (2007) P09012.

[30] G. Nicolis, Transformation properties of entropy production, Phys. Rev. E **83**, 011112 (2011).

[31] M. Esposito, Stochastic thermodynamics under coarse-graining, Phys. Rev. E **85**, 041125 (2012).

[32] S. Bo and A. Celani, Entropy production in stochastic systems with fast and slow time-scales, J. Stat. Phys. **154**, 1325 (2014).

[33] M. Santillán and H. Qian, Irreversible thermodynamics in multiscale stochastic dynamical systems, Phys. Rev. E **83**, 041130 (2011).

[34] K. Kawaguchi and Y. Nakayama, Fluctuation theorem for hidden entropy production, Phys. Rev. E **88**, 022147 (2013).

[35] S. Pigolotti and A. Vulpiani, Coarse graining of master equations with fast and slow states, J. Chem. Phys. **128**, 154114 (2008).

[36] A. Puglisi, S. Pigolotti, L. Rondoni, and A. Vulpiani, Entropy production and coarse graining in Markov processes, J. Stat. Mech.: Theor. Exp. (2010) P05015.

[37] B. Altaner and J. Vollmer, Fluctuation preserving coarse graining for biochemical systems, Phys. Rev. Lett. **108**, 228101 (2012).

[38] C. P. Amann, T. Schmiedl, and U. Seifert, Communications: Can one identify nonequilibrium in a three-state system by analyzing two-state trajectories? J. Chem. Phys. **132**, 041102 (2010).

[39] J. Mehl, B. Lander, C. Bechinger, V. Blickle, and U. Seifert, Role of hidden slow degrees of freedom in the fluctuation theorem, Phys. Rev. Lett. **108**, 220601 (2012).

[40] A. Crisanti, A. Puglisi, and D. Villamaina, Non-equilibrium and information: The role of cross-correlations, Phys. Rev. E **85**, 061127 (2012).

[41] A. Gomez-Marin, J. M. R. Parrondo, and C. Van den Broeck, Lower bounds on dissipation upon coarse-graining, Phys. Rev. E **78**, 011107 (2008).

[42] D. Tsygankov and M. E. Fisher, Kinetic models for mechanoenzymes: Structural aspects under large loads, J. Chem. Phys. **128**, 015102 (2008).

[43] D. Keller and C. Bustamante, The mechanochemistry of molecular motors, Biophys. J. **78**, 541 (2000).

[44] G. Lattanzi and A. Maritan, Force dependent transition rates in chemical kinetics models for motor proteins, J. Chem. Phys. **117**, 10339 (2002).

[45] G. Lattanzi and A. Maritan, Coarse grained models: The kinetics of motor proteins, Comp. Mater. Sci. **30**, 172 (2004).

[46] E. Gerritsma and P. Gaspard, Chemomechanical coupling and stochastic thermodynamics of the F1-ATPase molecuar motor with an applied external torque, Biophys. Rev. Lett. **05**, 163 (2010).

[47] P. R. Kramer, J. C. Latorre, and A. A. Khan, Two coarse-graining studies of stochastic models in molecular biology, Commun. Math. Sci. **8**, 481 (2010).

[48] H. Qian, The mathematical theory of molecular motor movement and chemomechanical energy transduction, J. Math. Chem. **27**, 219 (2000).

[49] S. Toyabe, T. Okamoto, T. Watanabe-Nakayama, H. Taketani, S. Kudo, and E. Muneyuki, Nonequilibrium energetics of a single F_1-ATPase molecule, Phys. Rev. Lett. **104**, 198103 (2010).

[50] K. Hayashi, H. Ueno, R. Iino, and H. Noji, Fluctuation theorem applied to F_1-ATPase, Phys. Rev. Lett. **104**, 218103 (2010).

[51] S. Toyabe, T. Watanabe-Nakayama, T. Okamoto, S. Kudo, and E. Muneyuki, Thermodynamic efficiency and mechanochemical coupling of F1-ATPase, Proc. Natl. Acad. Sci. U.S.A. **108**, 17951 (2011).

[52] R. Watanabe, K. Hayashi, H. Ueno, and H. Noji, Catalysis-enhancement via rotary fluctuation of F1-ATPase, Biophys. J. **105**, 2385 (2013).

[53] R. Yasuda, H. Noji, M. Yoshida, K. Kinosita, Jr., and H. Itoh, Resolution of distinct rotational substeps by submillisedcond kinetic analysis of F_1-ATPase, Nature **410**, 898 (2001).

[54] K. Adachi, K. Oiwa, T. Nishizaka, S. Furuike, H. Noji, H. Itoh, M. Yoshida, and K. Kinosita, Coupling of rotation and catalysis in F1-ATPase revealed by single-molecule imaging and manipulation, Cell **130**, 309 (2007).

[55] N. J. Carter and R. A. Cross, Mechanics of the kinesin step, Nature **435**, 308 (2005).

[56] M. J. Schilstra and S. R. Martin, An elastically tethered viscous load imposes a regular gait on the motion of myosin-V. Simulation of the effect of transient force relaxation on a stochastic process, J. R. Soc. Interface **3**, 153 (2006).

[57] T. L. Hill, *Free Energy Transduction and Biochemical Cycle Kinetics*, 2nd ed. (Dover, Mineola, NY, 1989).

[58] T. L. Hill, Studies in irreversible thermodynamics IV. Diagrammatic representation of steady state fluxes for unimolecular systems, J. Theor. Biol. **10**, 442 (1966).

[59] B. C. Carter, M. Vershinin, and S. P. Gross, A comparison of step-detection methods: How well can you do? Biophys. J **94**, 306 (2008).

[60] F. E. Müllner, S. Syed, P. R. Selvin, and F. J. Sigworth, Improved hidden markov models for molecular motors, part 1: Basic theory, Biophys. J. **99**, 3684 (2010).

[61] M. A. Little, B. C. Steel, F. Bai, Y. Sowa, T. Bilyard, D. M. Mueller, R. M. Berry, and N. S. Jones, Steps and bumps: Precision extraction of discrete states of molecular machines, Biophys. J. **101**, 477 (2011).

[62] U. Seifert, Stochastic thermodynamics of single enzymes and molecular motors, Eur. Phys. J. E **34**, 26 (2011).

[63] D. Hartich, A. C. Barato, and U. Seifert, Stochastic thermodynamics of bipartite systems: Transfer entropy inequalities and a Maxwell's demon interpretation, J. Stat. Mech.: Theor. Exp. (2014) P02016.

[64] N. Shiraishi and T. Sagawa, Fluctuation theorem for partially masked nonequilibrium dynamics, Phys. Rev. E **91**, 012130 (2015).

[65] A. Parmeggiani, F. Jülicher, A. Ajdari, and J. Prost, Energy transduction of isothermal ratchets: Generic aspects and specific examples close to and far from equilibrium, Phys. Rev. E **60**, 2127 (1999).

[66] H. Ge and H. Qian, Dissipation, generalized free energy, and a self-consistent nonequilibrium thermodynamics of chemically driven open subsystems, Phys. Rev. E **87**, 062125 (2013).